Master Thesis

Czech Technical University in Prague

F3

Faculty of Electrical Engineering
Department of Circuit Theory

Active power consumption meter

Bc. Tomáš Havel

Supervisor: Doc. Dr. Ing. Jiří Hospodka
December 2022

ZADÁNÍ DIPLOMOVÉ PRÁCE

I. OSOBNÍ A STUDIJNÍ ÚDAJE

Příjmení: **Havel** Jméno: **Tomáš** Osobní číslo: **474771**

Fakulta/ústav: **Fakulta elektrotechnická**

Zadávající katedra/ústav: **Katedra mikroelektroniky**

Studijní program: **Elektronika a komunikace**

Specializace: **Elektronika**

II. ÚDAJE K DIPLOMOVÉ PRÁCI

Název diplomové práce:

Aktivní měřič spotřeby elektrické energie

Název diplomové práce anglicky:

Active Electricity Consumption Meter

Pokyny pro vypracování:

Navrhněte zařízení pro měření spotřeby nízko příkonových elektronických obvodů (např. bateriově napájené aplikace). Mělo by dodávat elektrickou energii připojenému/měřenému zařízení, přičemž by mělo umožňovat monitorovat spotřebu tohoto zařízení a měřit/zaznamenávat i velmi krátké fluktuace ve spotřebě (např. přechodové stavy transceiverů apod.).
Základní vlastnosti měřiče:
- nastavitelné napájecí napětí pro měřené zařízení 1,8 V až 5 V s krokem 0,1 V, proud min. 0,5 A s ochranou proti přetížení,
- zobrazení hodnoty napětí a spotřeby na displeji (hodnoty max., min., avg atd.) s automaticky přepínaným rozsahy,
- funkce monitorování spotřeby včetně časové značky (následný přenos dat do PC),
- analogový napěťový výstup, jehož okamžitá hodnota napětí odpovídá okamžité spotřebě proudu.

Ověřte funkci a zhodnoťte dosažené výsledky.

Seznam doporučené literatury:

[1] Husák,M.: Napájecí zdroje v elektronice. Skriptum, ČVUT 2006
[2] Ripka, P., Tipek, A.(ed.): Modern Sensors Handbook. ISTE 2007, ISBN 978-1-905209-66-8
[3] Ziegler, S; Woodward, R. C.; Iu , H.C.,and Borle, L. J.: Current Sensing Techniques: A Review, IEEE Sensors Journal

Jméno a pracoviště vedoucí(ho) diplomové práce:

doc. Dr. Ing. Jiří Hospodka katedra teorie obvodů FEL

Jméno a pracoviště druhé(ho) vedoucí(ho) nebo konzultanta(ky) diplomové práce:

Datum zadání diplomové práce: **17.02.2022** Termín odevzdání diplomové práce: **10.01.2023**

Platnost zadání diplomové práce: **19.02.2024**

doc. Dr. Ing. Jiří Hospodka podpis vedoucí(ho) práce	prof. Ing. Pavel Hazdra, CSc. podpis vedoucí(ho) ústavu/katedry	prof. Mgr. Petr Páta, Ph.D. podpis děkana(ky)

III. PŘEVZETÍ ZADÁNÍ

Diplomant bere na vědomí, že je povinen vypracovat diplomovou práci samostatně, bez cizí pomoci, s výjimkou poskytnutých konzultací. Seznam použité literatury, jiných pramenů a jmen konzultantů je třeba uvést v diplomové práci.

. Datum převzetí zadání

Podpis studenta

Acknowledgements

Firstly, I would like to express my gratitude to Doc. Dr. Ing. Jiří Hospodka (CTU) for leading my thesis and providing beneficial support. As for the part of my study at NTUST, my dearest thanks to professor 邱煌仁 and doctor 張佑丞.

Secondly, I would also like to thank my family and friends for their support throughout the thesis creation.

Declaration

I hereby declare that I am the sole author and composer of my thesis and that no other sources or learning aids other than those listed have been used. Furthermore, I declare that I have acknowledged the work of others by providing detailed references of said work.

In Prague, 14. December 2022

Abstract

The aim of the thesis is to design a voltage regulator with adjustable output voltage while integrating a power consumption meter able to monitor fast and small current fluctuations. The thesis consists of a theoretical circuit design, an implementation of the device in the form of a printed circuit board, and final testing of all the functions of the implemented device.

The implemented device is able to provide 1.8 - 5 V (0.5 A) and acquire current samples with a high enough sampling frequency to capture pulses as shots as 5 µs. The obtained current samples show an average relative error of around 3 % in a wide range from 1 µA up to 0.5 A. Thanks to that, precise power consumption calculations with minimal, average, and maximal values are performed.

The calculated data can be either sent via USB to a computer, where a custom computer application receives and processes the data, or stored in an onboard FLASH memory for future acquisition. Moreover, when the device is connected to the computer, the implemented application allows user to adjust and control most of the device's functions. However, since the computer connection is not a necessity for the operation, the device can be controlled by onboard buttons with the measured data displayed on an included OLED display.

Keywords: Power consumption meter, current fluctuation, voltage regulator, analog-to-digital converter, microcontroller, printed circuit board

Supervisor: Doc. Dr. Ing. Jiří Hospodka
České vysoké učení technické v Praze
Fakulta elektrotechnická
Katedra teorie obvodů

Abstrakt

Tato práce se zabývá návrhem napěťového regulatoru s nastavitelným výstupním napětím a integrovným měřičem spotřeby, jenž je schopný detekovat rychlé a malé fluktuace odebíraného elektrického proudu. Součástí práce je teoretický návrh obvodu, realizace navrhnutého zařízení v podobě desky plošných spojů a následné otestování jednotlivých funkcí zařízení.

Realizované zařízení je schopné poskytnout 1.8 - 5 V (0.5 A) a zároveň zaznamenat měřené vzorky odběrového proudu s dostatečně vysokou vzorkovací frekvecí pro zachycení pulzů s délkou pouhých 5 µs. Vzorky naměřeného proudu vykazují průměrnou relativní odchylku okolo 3 % a to v širokém dynamickém rozsahu od 1 µA do 500 mA. Díky těmto hodnotám, přesná hodnota spotřeby elekrické energie je aktivně monitorována a minimální, průměrné a maximální hodnoty ukládány.

Tyto uložené hodnoty jsou pak následně buď zasláný s využitím USB konektoru do počítače, kde jsou přijata a zpracována navrženou aplikací, či uloženy ve FLASH paměti samotného zařízení pro budoucí zpracování. Uvedená počítačová aplikace zároveň uživateli dává možnost monitorovat měřené veličiny či nastavit a jednotlivé parametry zařízení. Jelikož připojení k počítači není požadavkem pro funkčnost zařízení, většinu nastavení a monitorování je možno provést pomocí dvou tlačítek a OLED displeje, které jsou součástí zařízení.

Klíčová slova: Měřič spotřeby energie, fluktuace elektrického proudu, regulátor napětí, analogově-digitální převodník, mikrokontrolér, deska plošných spojů

Překlad názvu: Aktivní měřič spotřeby elektrické energie

Contents

Figures

Tables

Abbreviations

LDO	Low-Dropout
AC	Alternating Current
DC	Direct Current
I^2C	Inter-Integrated Circuit
I^2S	Inter-IC Sound
SPI	Serial Peripheral Interface
CAN	Controller Area Network
USB	Universal Serial Bus
UART	Universal asynchronous receiver-transmitter
DAC	Digital-to-Analog Converter
ADC	Analog-to-Digital Converter
PWM	Pulse-Width Modulation
MOSFET	Metal-Oxide Semiconductor Field-Effect Transistor
SRAM	Static Random-Access Memory
SNR	Signal-to-Noise Ratio
PSRR	Power Supply Rejection Ratio
RC	Resistor–Capacitor
RLC	Resistor–Inductor-Capacitor
COM	Communication Port
GPIO	General-Purpose Input/Output
SCHEMATIC PINS	
REG_FB	DAC regulator adjustment signal
REG_EN	Regulator's enable signal
V_AD	Output voltage divided signal
MUX_FET	MOSFET and MUX digital switch signal
RS1_AMP	Output of RS1 amplifier
RS2_AMP	Output of RS2 amplifier
ADC_IN	Analog output of MUX, input for ADC
ADC_CNVST	SPI control signal for ADC
ADC_SDO	SPI data signal for ADC
ADC_SCLK	SPI clock signal for ADC
OSC	Oscilator output
DLO, CLK, RST	Signals for debugger
B	Button analog input
UART_TX	MCU's UART transmiter signal
UART_RX	MCU's UART receiver signal
I2C_SDA	I^2C SDA signal
I2C_SCL	I^2C SCL signal

Chapter 1

Introduction

In the last decades, there has been a massive increase in the production of low-power electronic devices. Even though tools like smartphones and battery-powered drills do not seem in any way similar, there is one thing that makes them much closer than one can realize. They are both battery-powered and require extreme power efficiency to satisfy customers' needs.

The trend of designing the majority of customer electronics battery-powered is recently very noticeable, and thus the need for low-power control is as crucial as ever. Nowadays, the circuitry is primarily digital and contains one or multiple microcontrollers or microprocessors. The power consumption of these computing integrated circuits is highly design dependent and cannot only be affected by simple microcontroller's sleep or standby modes but by, for example, lowering the refresh rate of a smartphone screen when the displayed image is idle [1]. However, using these adaptive methods, the power consumption may vary and while the device may consume only a couple of microamperes in sleep mode, sudden current consumption spikes may appear. For this reason, a reliable power supply with the ability to monitor small and fast current fluctuations is required to optimize the design.

This project non-directly follows up on my bachelor's thesis, where a battery management system (BMS) for 5 Li-Ion battery cells was designed. This protection system had to minimize the power consumption to preserve as much of the battery charge. The motivation and purpose of this paper is to construct a device that helps the designer to precisely measure power consumption, thus giving an ability to make necessary optimizations. Therefore, the paper proposes the design of an adjustable power supply with a precise power consumption meter for low-power applications (for example, battery-powered devices) featuring the ability to measure short current consumption fluctuations.

The paper is divided into three main sections; where the first section presents the design options for each component and sensor. The possibilities are briefly introduced with their respective advantages and disadvantages. The second section is dedicated to the design of a theoretically introduced circuit. This part is further divided into two main subsections, where the first focuses on the power supply, while the objective of the second part is to design the power consumption meter. The outcome of this part is the

completed circuit schematic. Based on the designed schematic, a printed circuit board is created in the last part, and measurements and results are presented.

Chapter 2

Theoretical background

2.1 Power and energy

Power, while omitting the power factor of alternating current, can be simply calculated as:

$$P = I \cdot V \tag{2.1}$$

The value of the consumed power should be provided in units of watts, respectively milliwatts or microwatts for low-power applications; however, as the power consumption is just the operating voltage multiplied by the current consumption, this can often be further simplified. This is most evident in circuits and components operating on a constant voltage level, resulting in the power consumption often being described only by units of milliamperes/microamperes [2].

The total energy consumption, with its main base unit being a joule [J] can then be described as the power consumption over a specific time period. In mathematical terms, this leads to the following integral:

$$E = \int_0^t P(t)\,dt \tag{2.2}$$

The energy consumption reading is often the value displayed by the household meters, while instead of the original unit – joule, it is in most cases substituted by a Wh, respectively kWh.

Knowledge of power consumption is essential not only for households and companies to keep track of their electricity bill but for battery-powered devices to provide as much operation time as possible on a single battery charge. For this purpose, power consumption meters are designed.

2.2 Power consumption meter

A power consumption meter, sometimes referred to as an electricity meter, is a device used to measure the power consumption of connected devices. Electricity meters are widely utilized and can be found almost in every single

household, monitoring the overall energy consumption of the property. These meters are often divided into three categories [3]:

1. Electromechanical induction meters

   The electromechanical meter is the most common analog type of energy meter used primarily to measure the energy consumption of a household. The meter includes a rotatory aluminum disc mounted between two electromagnets. Due to the induction of Eddy currents, the rotation of the disc is then proportional to the energy consumed.

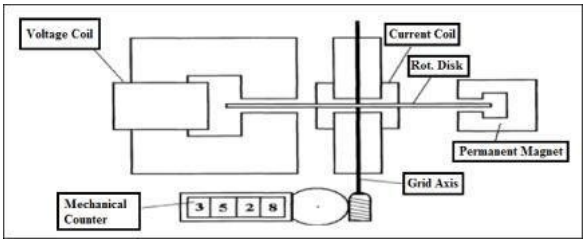

Figure 2.1: Electromechanical induction meter [4]

   However, these meters not only lack accuracy with the readings often in units of kilowatts, but they are also strictly designed for alternating currents.

2. Electronic energy meters

   As an electronic energy meter is considered a meter in which the analog rotary dial is substituted by an LED or LCD display. They can be either digital or analog, but they both usually combine some kind of current and voltage sensors followed by an analog-to-digital converter [5]. The main difference is that while in the analog version, the ADC is often followed by a frequency converter, the digital electronic meters utilize a processing unit that receives the data from individual sensors and processes them.

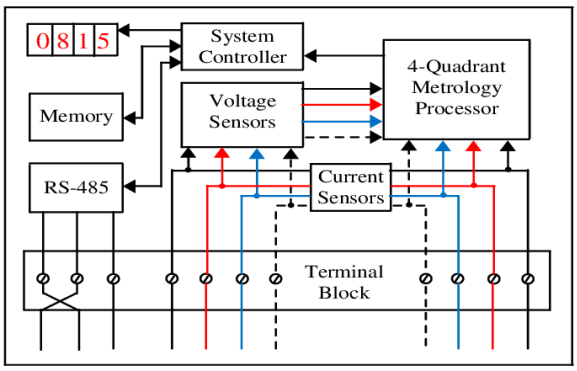

Figure 2.2: Digital electronic energy meter [5]

Electronic energy meters may utilize various sensors, and depending on the types of the sensors, they allow monitoring of alternating current but direct current as well. They can be designed to produce high-resolution measurements, allow to capture power consumption peaks (minimal, maximal values), and often include a memory to store these data.

3. Smart energy meters

   Smart energy meters do not bring any significant technological advancement, but they are mainly designed for the convenience of the energy provider. They often contain a similar set of sensors as electronic energy meters and provide similar functionalities. However, they most often utilize a specific secure communication protocol that directly connects the device with the provider. The energy consumption data are regularly transferred from the device to the control center, and thus no manual handling is needed. This is especially useful for the provider as it mitigates the possibility of power consumption tempering by the user. [5]

2.3 Building blocks

Even though the design approaches of an active power consumption meter may differ, multiple essential parts are needed. Firstly, to provide power to the device being measured, a stable power supply is needed. In case of a need for adjustable voltage output, circuitry allowing adjustability must be paired with the power supply. To calculate the power consumption, a voltage and current reading are necessary; thus, a presence of a voltage and current sensor is required. Lastly, the device needs a processing unit to transfer the data between sensors, respectively to allow data processing or superior system communication.

- stable power supply – 2.4
- output voltage adjustability – 2.5.1
- voltage and current sensors – 2.6
- digital control unit and communication interface – 2.7, 2.8

Each of the mentioned sections has multiple choices with their respective design methods, advantages, and disadvantages. To choose correctly, the following sections thoroughly introduce all the essential parts needed to construct an active power consumption meter while presenting their main features, as well as why and how they are used.

2.4 Voltage regulators

One of the most significant difficulties of many electronic circuits is designing a stable and low-noise power source. To choose the correct option for a specific design, this part of the thesis focuses on an introduction to several types of voltage regulators and DC/DC converters.

To fully understand the design, the beginning of this part presents the most common voltage regulator topologies with their respective working principle, capabilities, and properties. At the end of this part, multiple options for the adjustment of the voltage regulator's output voltage are introduced.

2.4.1 Linear regulators

As far as linear regulators are concerned, a variable resistance is usually introduced, resulting in a constant output voltage [6]. However, the input and output difference is dissipated as waste heat. Due to the structure, internal losses, and dropout voltages, the input voltage has to be consistently higher than the required output voltage.

Linear regulators are often the simplest types of voltage regulators and are usually categorized into two types according to the working principle.

Zener shunt regulator

The simplest type of linear voltage regulator is based on a Zener diode. A schematic of the Zener shunt regulator is shown in figure 2.3.

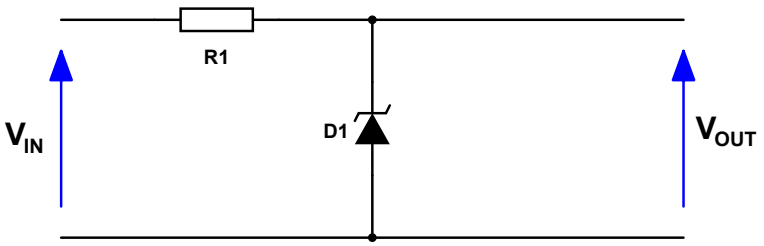

Figure 2.3: Zener diode shunt regulator (figure based on [7])

Even though the price and design complexity are very low, this voltage regulator has significant disadvantages. Firstly, when no load is connected, all the current will pass through the diode, potentially damaging it [8]. Secondly, the Zener current is dependent on many factors (temperature drift), thus not allowing a precise output regulation [7]. Lastly, this implementation offers no options for adjustability, and the output voltage is fixedly set during the design stage. The Zener shunt regulator is, for those reasons, used for very simple low-power applications, usually as a voltage reference.

Linear series regulator

In recent designs, the linear series voltage regulator is the most commonly used type of voltage regulator. Its applications range from simple low-power voltage references to power regulators with output currents reaching up to 10 A. Unlike the Zener shunt regulator, the series regulator introduces an active element, usually in the form of a transistor. The most basic structure is presented in figure 2.4.

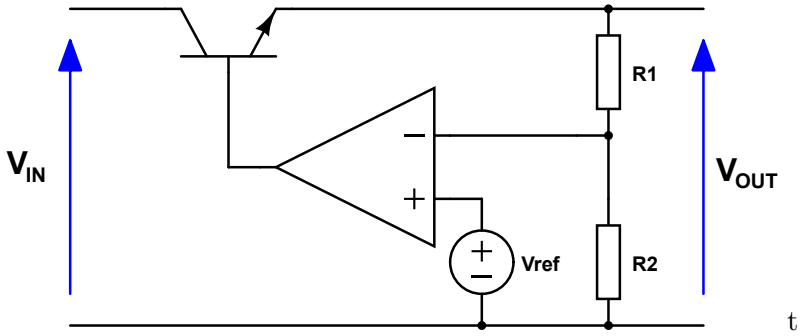

Figure 2.4: Linear series regulator (figure based on [9])

The structure usually consists of an error amplifier and a transistor acting as a variable resistor. Based on the output of the amplifier, a transistor (or network of transistors) is controlled, thus adjusting the output voltage [9]. Linear voltage regulators are known for their low cost, simple design, and low output noise. However, as stated before, they can only act as a step-down regulator, which means the output voltage is always lower than the input voltage. Therefore, the dropout voltage is inevitable in linear regulators, and even specialized low-drop-out regulators (LDO) always require input voltage tens to hundreds of millivolts higher than the output voltage.

2.4.2 Switching regulators

The second most common group of voltage regulators are switching regulators. Unlike linear regulators, their structure is usually more complex but comes with many advantages. Not only is their efficiency generally much higher, but based on the utilized topology, they can allow an output voltage higher than or the same as the input voltage. The switching regulators are divided into two categories [10]:

- Isolated switching regulators
- Non-isolated switching regulators

Isolated switching regulators

As the name suggests, the main difference is in isolation. The isolated switching regulators often use an inductor split to form a transformer, achieving galvanic isolation between the input and output [11].

Because the isolated switching regulators are mainly used either as an AC/DC converter or when a floating/level-shifted output is required, they are not described in this paper, and only the different types are stated below [12]:

- Flyback switching converter
- Forward switching converter
- Push-pull switching converter
- Full bridge switching converter

Non-isolated switching regulators

On the other hand, non-isolated switching regulators are widely utilized, and their understanding is needed for many DC designs. According to the requirements of the design, three topologies are the most common. They differ mainly in the relation between input and output voltage (decreasing, increasing), but their working principle is also slightly different. The three common topologies are:

- Buck (step-down) converter - $V_{IN} > V_{OUT}$
- Boost (step-up) converter - $V_{OUT} > V_{IN}$
- Buck-boost converter - $V_{OUT} <=> V_{IN}$

To successfully design a switching regulator, each topology's basic structure and principle must be understood. Because all of the previously stated topologies are closely similar and their basic structure consists of the same components, only with a different layout, in this section, only the Buck (step-down) converter is described in detail. If the main idea and principle are understood, most of the below-presented figures and equations can be easily transformed to suit the other two topologies.

Buck converter

A typical topology of a fundamental Buck converter is shown in figure 2.5.

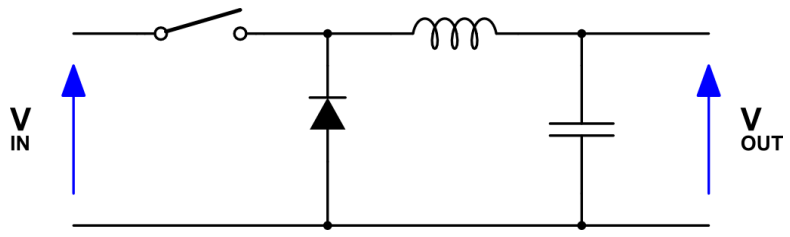

Figure 2.5: Basic topology of a buck converter (figure based on [13])

When the voltage at the input is applied, and the switch is closed, current flows through the inductor into the load. When the switch opens, the voltage

polarity on the inductor is reversed, and a closed loop consisting of a diode, inductor, and capacitor is created. Thus the output voltage is always less than or equal to the input voltage.

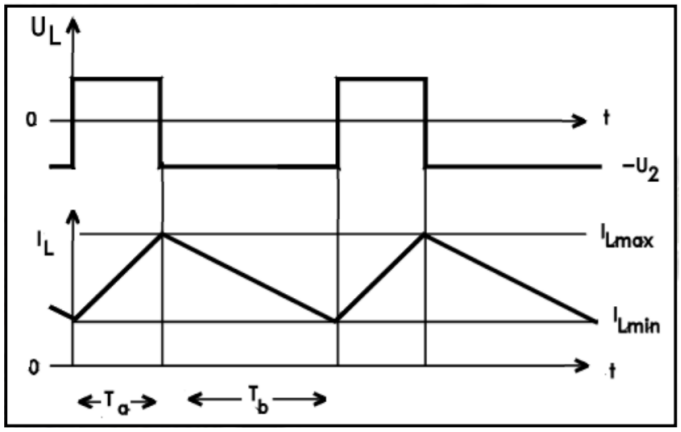

Figure 2.6: Behavior of voltage and current on the inductor [13]

The graph of the current through and voltage on the inductor shown in figure 2.6 not only presents a great visualization of the buck converter principle but can also be used to derive equations 2.3.

$$\Delta i_{L_a} = \frac{V_{IN} - V_{OUT}}{L} T_a \qquad \Delta i_{L_b} = \frac{V_{OUT}}{L} T_b \tag{2.3}$$

Putting the two expressions from 2.3 into equality, the following equation can be derived:

$$V_{OUT} = V_{IN} \frac{T_a}{T_a + T_b} \tag{2.4}$$

Even though the inductance itself is not present in the equation 2.4, if an equation of the output current is created, the inductance and the switching frequency play a significant role in the design.

Using expressions 2.3, equation 2.4 and the fact that $T_a + T_b = 1/f$, where f is the switching frequency, equations 2.5 stating the minimal required inductance can be derived.

$$T_a = \frac{V_{OUT}}{V_{IN} \cdot f} \qquad L = T_a \frac{V_{IN} - V_{OUT}}{\Delta I_L} \tag{2.5}$$

As the ΔI_L is unknown prior to an experimental measuring, it is often advised to approximate it as 20 % - 30 % of the maximal output current [14].

2.5 Integrated voltage regulators

Voltage regulators have been widely used and can be found in almost every electronic design. There can be tens to hundreds of voltage regulators in more complex designs. For that reason, there is a wide selection in the

form of a finished integrated circuit. These integrated circuits are usually well-optimized, offer good thermal and electric properties, and are often easier and cheaper to utilize.

Even though every regulator is different, they usually apply the same principle to determine the output voltage. Two types are often differentiated:

- Fixed-output voltage regulator – output voltage set by the manufacturer
- Adjustable voltage regulator – output voltage adjustable by the customer

While fixed-output regulators usually come in small packages and require only a few external components, the design of an adjustable voltage regulator is often a little bit more complicated but offers greater versatility.

2.5.1 Adjustable voltage regulators

The most common way to adjust the voltage regulator is by implementing a resistive feedback loop, as shown in figure 2.7. [15]

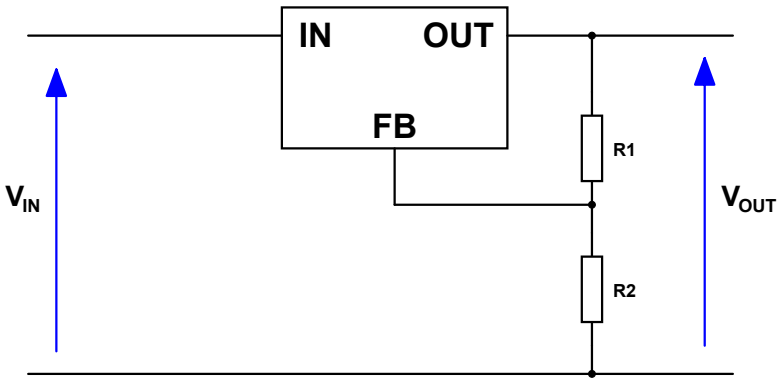

Figure 2.7: Diagram of regulator's feedback loop (figure based on [15])

Firstly, resistors R1 and R2 create a simple voltage divider producing a fraction of the output voltage on the regulator's feedback (FB) pin. Secondly, in the regulator itself, using an error amplifier, the input signal is compared to a reference voltage V_{FB}. This reference voltage is always stated in the respective voltage regulator's datasheet and depends on the type and manufacturer; however, the value is generally between 0.6 and 1.5 V. Finally, based on the differential error, either a duty cycle (switching regulator) or pass transistor state (linear regulator) of the regulator is adjusted, thus adjusting the output voltage. The output voltage can then be calculated as:

$$V_{OUT} = V_{FB}\frac{R1 + R2}{R2} \tag{2.6}$$

It can be observed that the output voltage is not dependent on the exact values of the resistors but on the ratio between their values. Even though this is partially correct, the resistance values play a significant role in the regulator's behavior. Lowering the value of R1 results in a higher quiescent current,

thus increasing the power consumption. On the other hand, decreasing the resistance often provides better output stability. A compromise between power consumption and stability is thus necessary [16].

While the output voltage can be adjusted using just the resistor network, in this arrangement, the adjustment is possible only before the service itself. In many hobbyist circuit designs, the resistor network is replaced by an analog potentiometer, enabling the adjustment while the system is operating.

2.5.2 Digitaly adjustable voltage regulator

Although the analog potentiometer seems like a simple and effective adjustment solution, digital adjustment is necessary for some designs. The following section focuses on many possible digital adjustment methods used to adjust the regulator's output voltage using a microcontroller or similar type of control circuit.

Voltage regulators with communication interface

Lately, there has been a development of voltage converters with a built-in communication interface. This option seems like a great solution that usually offers good properties and stability while making the hardware design extremely simple without needing an external adjustment solution.

Although it seems there are no disadvantages of using a converter like this, when the design requires adjustment during the operation, the main disadvantage is the availability. Firstly, since this technology has not been manufactured for a long time, there are limited choice options and limited stock with an extended delivery lead time. Secondly, the integrated circuits often provide a fixed output voltage adjustment step (usually around 20 mV) that may not be sufficient in some designs.

To give an example, there are some options for buck converters with I2C interface from Texas Instruments (specifically TPS65263RHBT [17] or TPS628501DRLR [18]) as well as options from Microchip Technology (specifically MIC33M356 [19] or MIC24045 [20])

Digital rheostat/potentiometer

Another option is replacing the entire or part of the resistor feedback network with a digital potentiometer or digital rheostat. A possible design of a system with digital I^2C controlled rheostat is presented in figure 2.8.

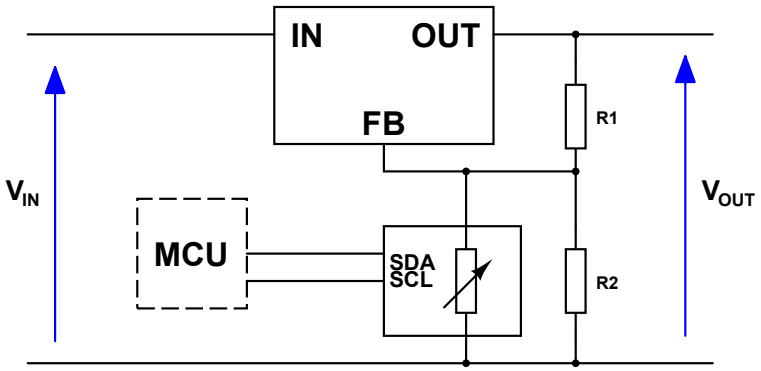

Figure 2.8: Adjustable regulator using digital rheostat (figure based on [21])

It shall be noted that the system should be designed in a way that considers the possibility of the digital rheostat behaving as an open circuit occurring before a startup of the device. Thus there should always be another resistive path parallel to the rheostat [21].

As in the equation 4.9, the output can be simply derived as:

$$V_{OUT} = V_{FB}\frac{R1 + (R2 \parallel R_{RH})}{(R2 \parallel R_{RH})} \tag{2.7}$$

Solution 2.8 is simple and presents almost no intervention to the regulator's stability. On the other hand, the tolerances of digital potentiometers, as well as the rheostats, are often poor, and the percentage of error in the resistance is usually around 20% [22]. Lastly, the adjustment step of the output voltage is non-linear and follows exponential growth.

On the graph 2.9 this nonlinear dependence is presented using schematic 2.8, equation 2.7, a 256-position digital rheostat and following parameters:

$$R1 = R2 = 15\,\mathrm{k\Omega} \qquad R_{RH} = 0 - 10\,\mathrm{k\Omega} \qquad V_{FB} = 0.6\,\mathrm{V} \tag{2.8}$$

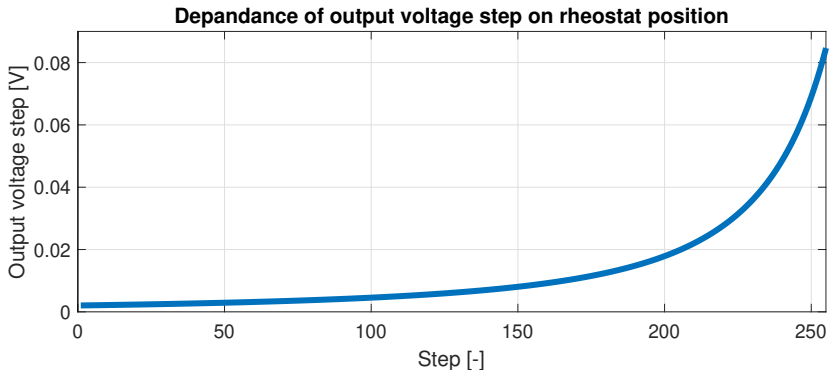

Figure 2.9: Non-linear output voltage dependance

Digital to analog converter

An alternative commonly utilized method to digitally adjust the output voltage is the implementation of a digital-to-analog converter. The method is based on an additional signal fed to the feedback pin through a resistor [23].

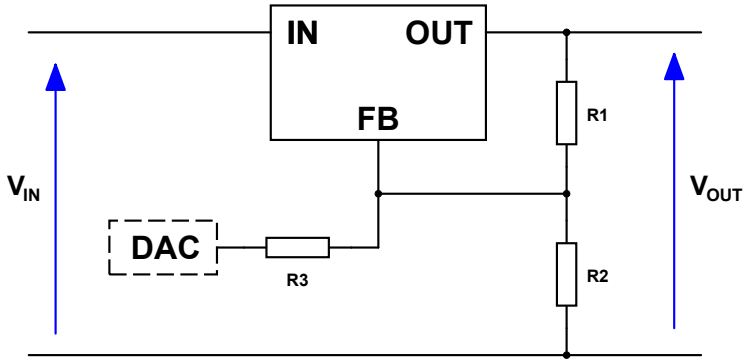

Figure 2.10: Adjustable regulator using DAC signal (figure based on [23])

To calculate the output voltage using an additional DAC signal, an equation 2.9 is used.

$$V_{OUT} = V_{FB}(1 + \frac{R1}{R2}) - \frac{R1}{R3}(V_{DAC} - V_{FB}) \tag{2.9}$$

The signal source can either be an external digital-to-analog converter or an internal DAC integrated into most conventional microcontrollers. For this purpose, specialized current-mode DACs are available; however, they are usually much more expensive. Even though the use of a current DAC may result in better performance, a standard DAC with voltage output can be coerced in service simply by putting a resistor between the output of the DAC and FB node – in the case of schematic 2.9, resistor R3 [24].

This method mitigates the non-linear adjustment step and, combined with a microcontroller, presents a solution requiring a minimum number of external components.

PWM

The last presented method is very similar to the previously described adjustment solution (2.5.2).

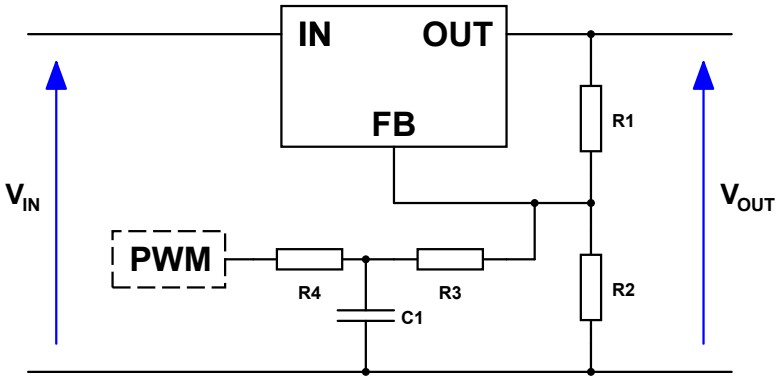

Figure 2.11: Adjustable regulator using filtered PWM (figure based on [25])

The working principle shown in figure 2.11 is closely similar to the digital-to-analog converter method, but instead of the DAC, pulse-width modulation is utilized. This solution is optimal for designs using a microcontroller without an integrated DAC but with a PWM signal for disposal [25]. However, an additional RC filter is required to filter the PWM signal and supply a stable voltage to the feedback pin. Moreover, the frequency of the PWM signal may appear on the output rail, or issues arising from the variation in the PWM signal's RC filter over the temperature range may occur [23].

2.6 Current sensor

As far as a current sensor is concerned, multiple options are commonly available. Since the paper focuses on DC measurements, all the below-mentioned options are able to measure the DC. However, as it is with all component choices, no option is perfect in every aspect, and compromises have to be made.

2.6.1 Current sensors based on Ohm's law

The principle of these direct current sensing methods originates in Ohm's law, that states:

$$I = \frac{V}{R} \tag{2.10}$$

where:

I is the current through the conductor
V is the voltage measured across the conductor
R is the resistance of the conductor

This relation clearly states that to derive the current through the conductor while the resistance is known, only voltage measurements have to be taken.

This transforms the required current sensor into a voltage sensor, which is generally much easier and simpler to design and utilize.

A common approach is the use of a current-sensing shunt resistor. A measured voltage drop on the resistor is proportional to the required current value. Thus, these sensors often offer a low-cost, reliable solution thanks to their simple structure. However, the shunt resistor is placed in the current flow's direct path, causing the mentioned power loss and thus limiting the possible usage and applications.

High-performance coaxial shunt

When it comes to a direct Ohm's law-based methods, one of the most accurate options is a coaxial shunt.

In current sensing shunt resistors, the position and length of the sense wires are crucial. Moreover, the sense wires introduce a parasitic inductance that can significantly influence the performance. Hence, for a high-performance application, a coaxial shunt is designed and is presented in figure 2.12.

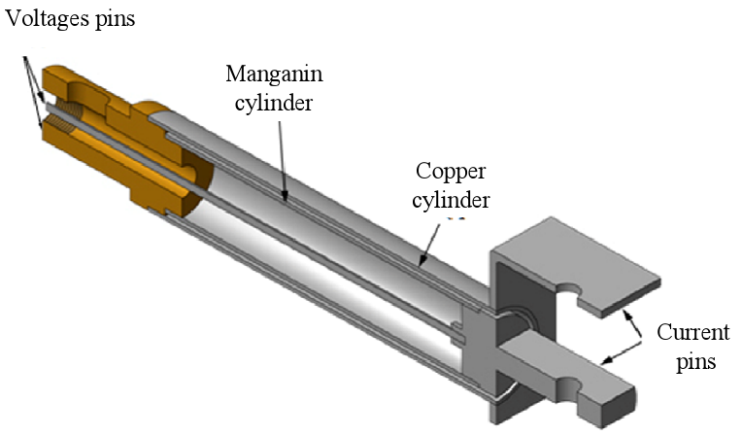

Figure 2.12: Coaxial shunt resistor [26]

The presented structure significantly reduces the parasitic inductance by reducing the flux that couples into the sense wires, hence making the coaxial shunt ideal for high-frequency applications [26]. However, the structure is bulky and unsuitable for small integrated designs.

Surface-mounted shunt resistor

While the coaxial method offers some excellent properties, the form factor disadvantage in many designs outweighs the advantages. For that reason, a surface-mounted shunt resistor is present in a majority of electronic devices.

However, with relatively small integrated shunt resistors, an equivalent circuit model must be accounted for. This is especially important when working with alternating current or high-frequency pulses.

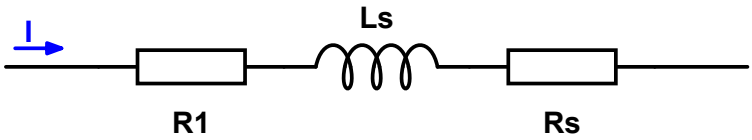

Figure 2.13: Shunt resistor – equivalent circuit (figure based on [27])

In the circuit 2.13 multiple parasitic parameters are present. L_s is the parasitic inductance, R_s is the parasitic resistance due to skin effect and R is the nominal resistance [27]. Thanks to the small size of surface-mounted shunt resistors, the skin effect becomes negligible, hence the cutoff frequency can be derived as:

$$f_c = \frac{R}{2\pi L_s} \tag{2.11}$$

Secondly, the thermal drift of the shunt resistor may be noticeable and cause undesired measurement deviations. These inaccuracies can be partially suppressed by material, size, or by utilizing proper sense wire connection. Hence, most of these resistors are slightly larger and thicker than conventional surface mount resistors and often implement four-terminal connections with two pairs of separated connections for the current path itself and the sense wires. The four-terminal resistor can be observed in figure 2.14.

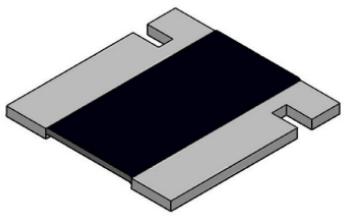

Figure 2.14: 4-terminal shunt resistor [28]

An alternative to a four-terminal current sense resistor is a correct printed circuit board layout with a Kelvin connection. This measuring technique separates the current-carrying path from the current sensing path. One of the possible layouts with standard two-terminal resistors is shown in figure 2.15

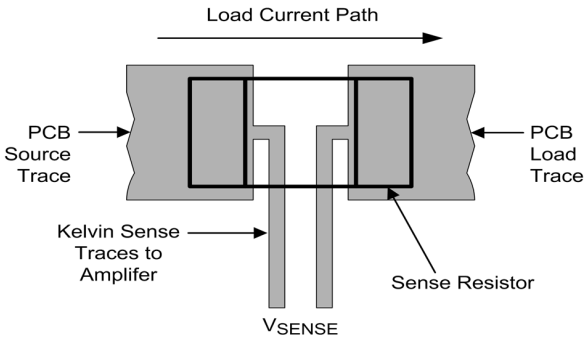

Figure 2.15: Current sense resistor – Kelvin's connection [29]

This solution is relatively low-cost (around 1 USD) and provides a reliable and decently accurate option for integrated designs. However, as with the coaxial shunt resistor, a power loss on the resistor is inevitable. Therefore, by choosing the resistance value, a compromise between low power loss and sufficient accuracy must be made.

Trace resistance sensing

Instead of a shunt resistor, an intrinsic resistance of copper trace may be used for current sensing. This approach offers an extremely low-cost solution without needing a shunt resistor while not introducing additional power loss to the circuit. However, because of the copper trace's small resistance, the resulting voltage drop is minimal and needs massive amplification to produce sufficient signal strength. Furthermore, copper exhibits strong thermal dependence, and thus the thermal drift significantly affects the accuracy of this method [30].

Since the only advantage of this method is mainly its low cost, it is not commonly utilized and is not suitable for applications where accuracy is required.

2.6.2 Hall current sensor

Typically when an electric current flows through any material, the electrons generally move in a straight line. However, when a conductor with a flowing current is placed in an external magnetic field, the field exerts a transverse force on the moving charge carriers, which tends to push them to one side of the conductor [31]. This effect is called a Hall effect and is most evident in wide and flat conductors as shown in 2.16.

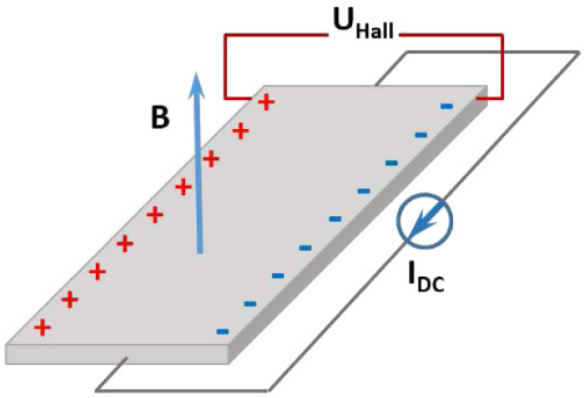

Figure 2.16: Working principle of Hall current sensor [32]

Because of the electron buildup on one side of the material, a potential difference will then appear, and the Hall voltage – U_{Hall} can be measured. The Hall voltage satisfies the following equation. [33]

$$V_{\text{Hall}} = I \cdot B \cdot k \tag{2.12}$$

where:

I is the current flowing through the conductor
B is the magnetic flux density cause by the magnetic field
k is a constant corresponding to material type and thickness

Although these types of sensors used to be large, bulky, and unsuitable for integrated applications, recently, many Hall sensors in compact surface-mounted packages started to appear.

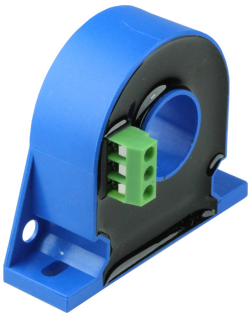

(a) : Older, bulky type (up to 100A) [34]

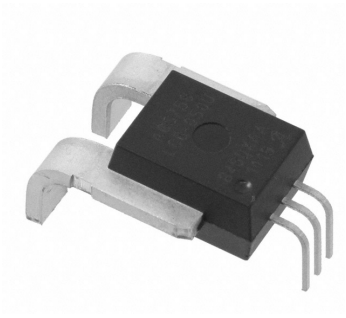

(b) : Small, compact (up to 50A) [35]

Figure 2.17: Commercially available Hall current sensors

Unlike Ohm's based methods, this indirect solution offers a current reading without introducing a power loss to the circuit. However, these sensors suffer from a significant temperature drift and voltage offset present even without flowing current.

2.6.3 Fluxgate current sensor

A fluxgate sensor is another example of an indirect current sensor based on a magnetic field. The structure of the fluxgate current sensor is usually much more complicated than previously described methods.

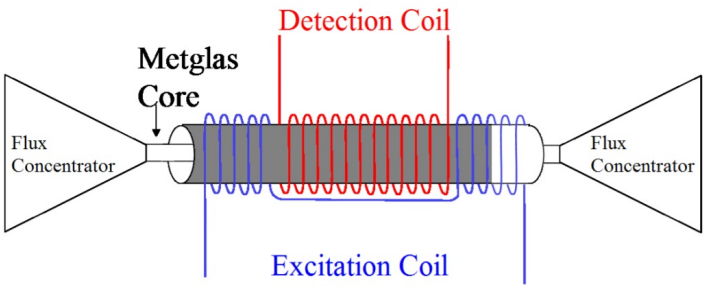

Figure 2.18: Typical design of a fluxgate magnetometer [36]

The structure, as shown in figure 2.18, usually consists of a highly permeable core and two coils. The basic working principle of a fluxgate sensor is about the periodic change of the magnetic permeability of the soft ferromagnetic core, which is driven by a periodic exciting current. The exciting current will induce a magnetic field in the core and thus also induce a current in the sensing coil winding. When no external magnetic field is present – no current is flowing, the current of the exciting windings and the sensing windings matches. However, when a flowing current is introduced, an additional magnetic field is induced, the core becomes more easily saturated in one direction. Thus the currents of the exciting windings and the sensing windings will no longer match. [37]

Their performance is said to be up to twenty times better than Hall-effect current sensors [38]. However, they are usually more expensive, larger, and require more external circuitry.

2.6.4 Comparison

In the previous part, the three most common current sensors were introduced. Each of the options has its respective advantages, disadvantages, and suitable application. To make a correct choice, a table comparing the properties of the presented methods is shown in (2.1) with some key features below.

	Type	Accuracy	Thermal drift	Range	Bandwidth
Coaxial	direct	0.1-1%	10-12 ppm/°C	A - kA	MHz - GHz
SMT shunt	direct	0.2 - 2%	20 - 200 ppm/°C	µA - A	kHz - MHz
Trace	direct	1-5%	3900 ppm/°C	A - kA	kHz
Hall	indirect	0.5 - 5%	50 - 1000 ppm/°C	A - kA	kHz
Fluxgate	indirect	0.001 – 0.5%	$<$ 50 ppm/°C	mA - kA	kHz

Table 2.1: Comparison of current sensing methods [39, 40, 41, 42]

It is important to say that values presented in table 2.1 are only approximate, and there can definitely be a current sensor of a specific type that is out of stated bounds. Furthermore, the values are highly dependent on the individual choice, where a 1 Ω shunt resistor will indeed display different properties than a 1 mΩ resistor. For this reason, a list shortly summarizing the main advantages and properties of each type was created:

- Coaxial shunt – good accuracy and frequency bandwidth, bulky, relatively expensive
- Surface-mounted shunt – simple, small, decent accuracy and frequency bandwidth, cheap
- Trace resistance sensing – minimum additional components, extremely cheap, strong thermal drift, non-ideal accuracy
- Hall sensor – no direct power loss, decently accurate
- Fluxgate sensor – no direct power loss, extremely accurate, more difficult to utilize, relatively expensive

2.6.5 Dynamic ranging

Many applications require accurate current measurements over a wide range. This can range from units of nanoamperes up to tens of amperes. Maintaining accuracy within such a wide dynamic range may prove challenging, and a single current sensor from the above-described options may not be sufficient.

To provide an accurate reading over a wide range, auto-ranging methods are introduced, enabling dynamic adaptation during the running measurement. This is especially important for Ohm's law-based methods, where a resistance value selection that satisfies the maximum power loss requirements may not meet the accuracy needs.

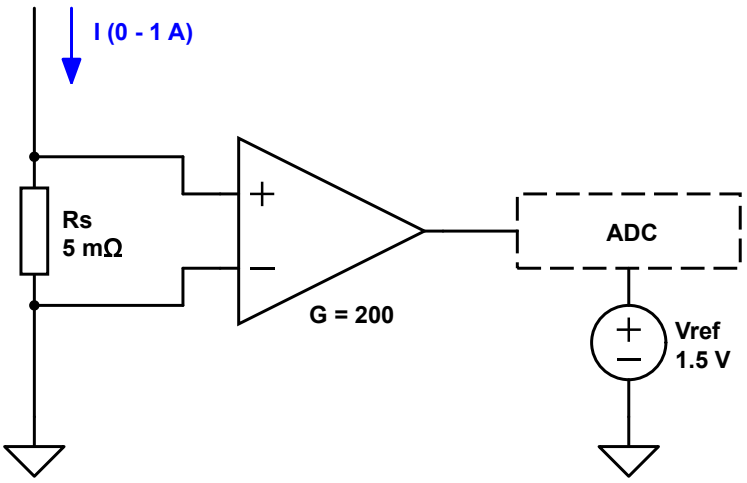

Figure 2.19: Current sensor – based on shunt resistor (figure based on [43])

This problem can be demonstrated by circuit example 2.19. Considering a 16-bit analog-to-digital converter with a 1.5 V voltage reference and a 5 mΩ shunt resistor with 200 V/V gain amplifier, a minimal measurable current is derived as:

$$I_{res} = \frac{\frac{V_{ADCref}}{ADC_{res}} \cdot \frac{1}{G}}{R_s} = \frac{\frac{1.5}{2^{16}} \cdot \frac{1}{200}}{0.005} \sim 23\,\mu\text{A} \tag{2.13}$$

Since this resolution may be insufficient for some applications, an idea of increasing the resistance value of the shunt resistor or amplifier gain may occur. However, an increase in the resistance introduces more significant power loss. Furthermore, considering a gain of 1000 and current flow of 1 A, an output voltage of the amplifier can be derived as:

$$V_{AMPout} = R_s \cdot I \cdot G = 0.005 \cdot 1 \cdot 1000 = 5\,\text{V} \tag{2.14}$$

This value is clearly out of the ADC bounds, thus increasing the low-current accuracy but making a higher current measurement impossible. This problem has two commonly known solutions.

Current shunt switching

As a first solution, a current shunt switching method is implemented (figure 2.20).

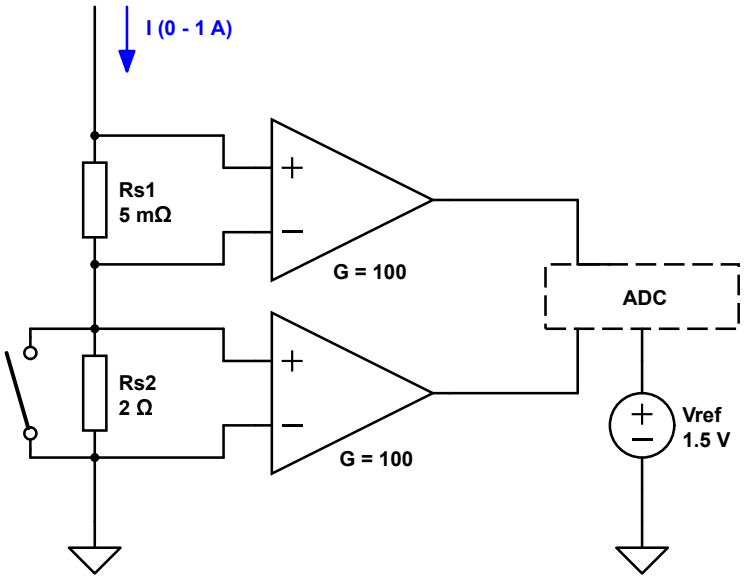

Figure 2.20: Current shunt switching technique (figure based on [43])

The accuracy improvement is achieved by utilizing a second serial shunt resistor with a different value. A bigger shunt resistor can be used for smaller currents, while a smaller resistor is used for larger currents. Although, placing another resistor in the current path causes more significant power losses.

Hence a low ON-state resistance switch is placed parallel to the larger resistor, bypassing the high-resistance path as soon as higher currents are detected [43].

This method is suitable for applications requiring high accuracy without too much additional power loss. Moreover, this method is scalable by simply using more serial resistors with different values while bypassing every additional resistor with a bypass switch.

On the other hand, the designed circuit is usually more expensive and complex with a need of multiple differential amplifiers, low ON-state resistance switches, and either a multiple-channel ADC or a signal multiplexer.

Logarithmic amplifier

If space or price is a big concern, a logarithmic amplifier might be a viable option. The logarithmic amplifier (basic diode structure shown in figure 2.21) is in a circuit used as a regular operational amplifier; however, it brings some advantages.

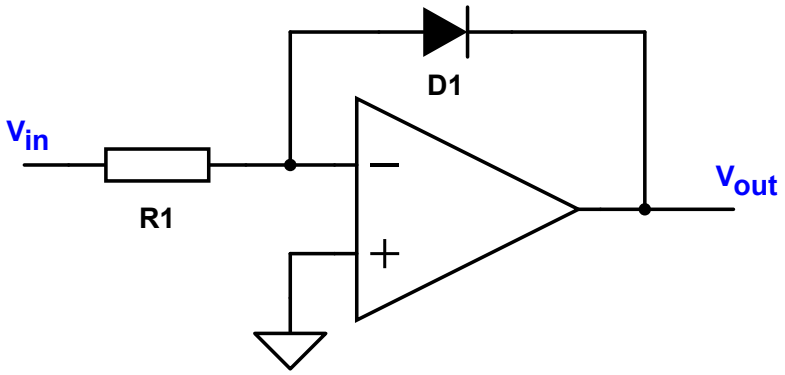

Figure 2.21: Logarithmic diode amplifier (figure based on [44])

Unlike an operational amplifier, where the output is equal to the amplified voltage difference between the inputs, a logarithmic amplifier outputs a signal that is proportional to the logarithm of the applied input [44]. This dependence can be derived as: [45]

$$V_{OUT} = -V_T \ln \frac{V_{IN}}{I_S \cdot R1} \tag{2.15}$$

where:

I_S is saturation current of diode D1
V_T is thermal voltage of diode D1

As the logarithmic dependence suggests, when the input voltage is low, the amplification coefficient is much higher than when the input voltage is higher, as shown in figure 2.24.

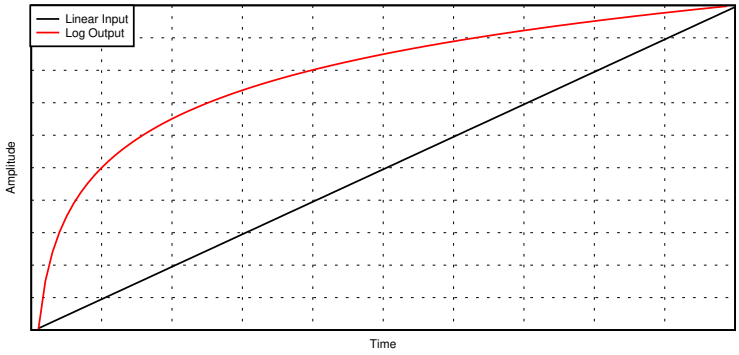

Figure 2.22: Logarithmic diode amplifier – input-output dependancy [46]

While this seems like a perfect solution for a wide dynamic range, the logarithmic amplifier has many crucial disadvantages. Firstly, a disadvantage evident from 2.21 is the absence of differential inputs, hence accepting only unipolar signal and making this option suitable only for low-side current sensing. Secondly, the logarithmic amplifiers are known for high-temperature dependence and a significant reduction of signal-to-noise ratio (SNR) [45, 47].

2.6.6 Voltage signal evaluation

Even though the presented options are in many ways different, their job is almost always to transfer the current reading into an easily measurable voltage output. The solution then requires a precise sampling circuit to process the reading.

In most systems, the voltage reading is processed by an analog-to-digital converter. This can be achieved either by an integrated ADC in the utilized microcontroller or an external ADC, sending its measured data via a communication interface (usually SPI) to the superior system.

When choosing the right ADC for the application, multiple parameters have to be paid attention to. The most significant for the majority of applications are [48]:

- Conversion resolution
  - provided as X-bit, where X is 8, 12, 16 etc.
  - refers to the number of output bits that the ADC can generate per conversion
- Conversion speed
  - provided in units of *sps* (samples-per-second)
  - refers to the maximum number of conversions per second
- Accuracy and noise
  - combination of multiple parameters

- usually SNR (signal-to-noise ratio), THD (total harmonic distortion), DNL (differential nonlinearity) and many others

On top of that, the available selection of analog-to-digital converters is pretty wide and usually divided into five categories. The categories are presented below with a short introduction and the most significant properties. [49]

- Flash ADC - extremely fast (up to 10 Gsps), lack resolution (generally limited to 8-bit)
- Successive Approximation (SAR) - cheapest, slower (up to 10 Msps), higher resolution (up to 18-bit)
- Delta-sigma (Δ-Σ) - slowest (up to 1 Msps), highest resolution (up to 32-bit)
- Pipelined - functionally similar to SAR, the middle ground between SAR ADC and Flash ADC (up to 10 Gsps, up to 16-bit)
- Dual Slope - high resolution, high accuracy, very slow sampling rate

According to the application, a suitable type with suitable parameters must be chosen to achieve the required results.

2.7 Control unit

As a majority of current electronic devices require data collection, data storage, or commutation with a superior system, the presence of a digital computing unit is often inevitable. Multiple options arise depending on the level of integration, computing requirements, and cost.

2.7.1 Single board control circuits

When a design is not planned to be mass-produced and does not require industrial-grade protection and shielding, commercially available microcontroller boards or single-board computers are a solid option. These boards are usually user-friendly and include many universal interfaces. On top of that, programming is often straightforward, with many included libraries and examples. As an example of a microcontroller board, Arduino boards cannot be omitted, while as the representative of single-board computers, a series of Raspberry Pi boards are widely known.

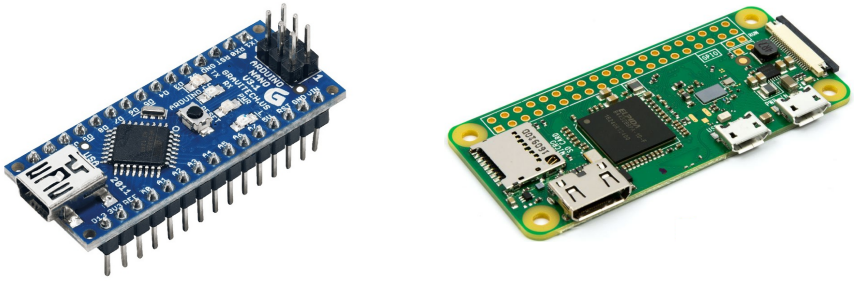

(a) : Arduino Nano [50] **(b) :** Raspberry Pi Zero [51]

Figure 2.23: Single board control circuits

Even though these boards are generally considered hobbyist boards and entry-level to electronics, Arduino and Raspberry Pi boards are currently being used in many commercial and even industrial applications [52].

2.7.2 Single chip microcontrollers

When space and price are a big concern, a single-chip microcontroller unit can be included in the circuit design. Firstly, only one compact printed circuit board can be created, including all the required circuitry as well as the microcontroller itself. Secondly, many microcontrollers feature sleep or standby modes and, when well optimized, can operate with minimal current consumption reaching only units of μA. Lastly, there has been a massive improvement in the features and properties of microcontroller units in the last decade. These chips not only contain powerful processing cores but usually comes along with memory, communication interfaces, and many programmable inputs and outputs.

To present how powerful a single chip microcontroller can get, an example of STM32H723/733 [53] is given.

Figure 2.24: STM32H723/733 in LQFP100 package [54]

This integrated circuit with a footprint of only 8 mm x 8 mm in TFBGA100

package introduced in 2020 by STMicroelectronics is a very high-performance device that provides most of the necessary functions and features for the majority of electronic devices. It features: [53]

- up to 550 MHz operating frequency, up to 2 MB of Flash memory
- up to 3.6 Msps ADC with 16-bit resolution
- up to 1 Msps DAC with 12-bit resolution
- up to 35 communication interfaces (UART, I2C, SPI, USB etc.)

Although the STM32H723/733 is an excellent example of recent technological advancement, for most applications, a microcontroller this powerful is unnecessary, and the price tag of around US$20 is often hard to justify.

However, there is a vast selection of various microcontrollers from multiple manufacturers (Microchip Technology, NXP, STMicroelectronics) offering different speeds, interfaces, and features. To contrast the US$20 STM32H723/733, lower-performance microcontrollers that can satisfy most basic designs can be found for as low as US$1. As an example of widely known mid-range microcontrollers, Atmel SAMD21 [55] series have to be mentioned.

When choosing the microcontroller for the respective design, depending on the application, multiple things have to be first considered.

2.8 Communication interface

If either the single-board computer or the microcontroller itself is selected, communication with other devices is often required. The communication needs may range from sensor-to-sensor communication up to communication with a superior system like a computer.

2.8.1 Superior system communication

To actively monitor the current consumption, an implementation of a communication line between a computer and the control circuit of the design is necessary. The microcontroller usually conducts this communication, sending the measured data to the computer. The recent microcontrollers often offer many communication interfaces usable for superior system communication like:

- USB - universal serial bus, primarily used peripheral connection between the circuit and the computer
- UART - serial interface, providing easy and simple communication between parts of the circuit, but is widely utilized for communication with computer

The following options arise as the most suitable interfaces for the required communication with a superior system.

RS-232

Communication standard RS-232 offers a simple software implementation using the UART interface. Moreover, if the application requires an industrial-grade connection, the RS-232 usually implements a sturdy connector D-SUB DE-9 [56]. Even though the connector is made to withstand industrial needs, it is nearly impossible to connect it to a computer nowadays. This solution is thus suitable when communication with an older industrial machine is required rather than a personal computer.

USB

If a connection to a computer is the number one priority, the universal serial bus with its widely used connectors is the ideal solution. However, successfully implementing a software part of USB protocol can sometimes be challenging and requires deep programming knowledge.

UART-USB converter

To simplify the software part but keep the user-friendly USB connector, UART-to-USB converters are often used. This either one chip converter (2.25a) or a finished single board system (2.25b) converts the UART logic levels to the logic levels required by the USB. In a computer, the device is then usually detectable as a virtual COM port [57].

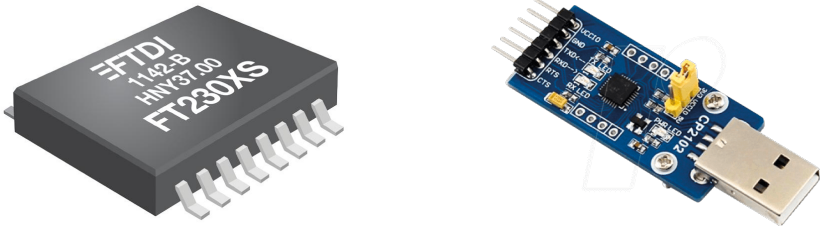

(a) : Single chip – FT230XS [58] **(b) :** Manufactured USB dongle [59]

Figure 2.25: UART-to-USB converter

2.8.2 Sensor and user interface communication

When a data transfer between the control unit (microcontroller) and the superior system (computer) is resolved, getting the necessary data from sensors to the respective control circuit is needed. Hence, the following communication interfaces are the most common and widely utilized to connect various peripherals chips to the primary control circuit.

SPI

A serial peripheral interface or SPI is an example of a communication interface invented in 1979 by Motorola. Since then, it has become widely popular

and standardized. The SPI is a high-speed, full-duplex, synchronous serial input/output port that allows a serial bit stream of programmed length (2 to 16 bits) to be shifted into and out of the device at a programmed bit-transfer rate [60].

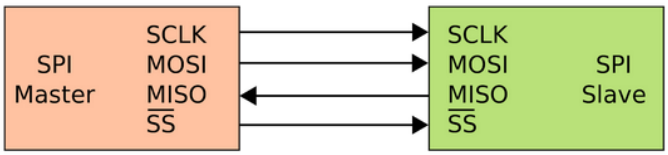

Figure 2.26: SPI communication interface [61]

As shown in figure 2.26, SPI interface usually consists of a 3-wire connection (clock signal, input data stream, and output data stream), plus a slave select pin is required. Moreover, an SPI master must have as many slave select outputs as the number of connected slaves, which may cause troubles in designs with many peripheries. However, the SPI interface is well-optimized for high speeds and is ideal for communication with a single ADC, SRAM, or other high-speed demanding peripheries.

I²C

When speed is not the primary concern, the I²C communication interface presents itself as a viable option.

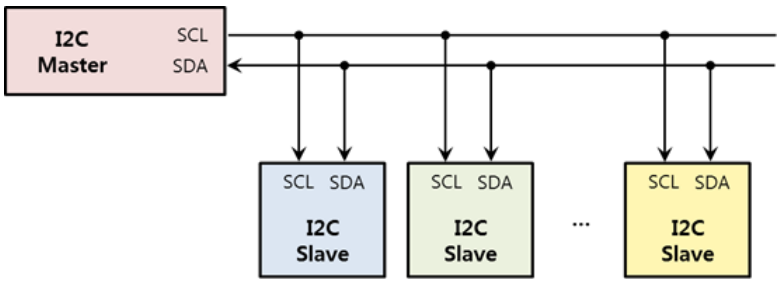

Figure 2.27: I²C communication interface [62]

Unlike with SPI, in the case of the I²C interface, only two wires are needed for communication. The lack of a slave select signal present in SPI is resolved by sending an address byte before each data byte and allowing huge scalability with up to 127 simultaneously connected slaves. However, it significantly decreases the speed capabilities [63]. For these reasons, the I²C interface is usually utilized for small displays, temperature sensors, and other non-demanding peripheries.

When creating a design with an I²C interface, it shall not be forgotten that both lines (SDA, SCL) are required to have a pull-up resistor.

CAN

In 1983 BOSCH developed a CAN bus as a multi-master message broadcast system that specifies a maximum signaling rate of 1 megabit per second (bps). The communication protocol is reliable and robust and was initially designed for automotive use. Unlike the previous interfaces, the CAN bus is designed so all connected devices and peripherals can listen simultaneously and send data independently of each other. This independency may result in transmission collisions, which are resolved by assigned priority token [64].

Chapter 3

Own solution proposal

Before the design itself, it should be mentioned that most of the project was created in the years 2021 and 2022 during the COVID-19 pandemic. Not only did this affect the ability to use laboratories and other facilities, but also, due to the massive semiconductor shortage, local electronic stores usually did not offer a wide selection of the respective component. In some cases, even the most essential components were hard to obtain. This shortage resulted in a more significant need for compromise than anticipated, and some components had to be chosen only because no other options were available.

The chapter is divided into seven subsections. While the first two introduce the assignment, the following four sections focus on the respective part of the circuit required for the power consumption meter. In the last section, the proposed circuit's output capabilities are summarized.

3.1 Assignment

As mentioned at the beginning of the paper, a goal was to design a power consumption meter with the ability to monitor small and fast current peaks. The required parameters and capabilities are in detail described in the following list:

- the power consumption meter is connected as a voltage power supply to the measured device
- adjustable output voltage in a range from 1.8 V to 5 V with a 0.1 V step size
- output current at least 0.5 A
- overload protection
- automatic current measurement range switching
- ability to measure currents as low as units of microamperes and fast current pulses in lengths of tens of microseconds.
- output voltage and power consumption displayed on display – with minimal, maximal, and average values

- power consumption readings stored with a respective timestamp
- analog output – voltage reading corresponds to the current consumption – used for oscilloscope connection

3.2 Design analysis

To design individual subcircuits of the device, a block diagram was created. Figure 3.1 shows the individual building blocks needed to satisfy the design requirements.

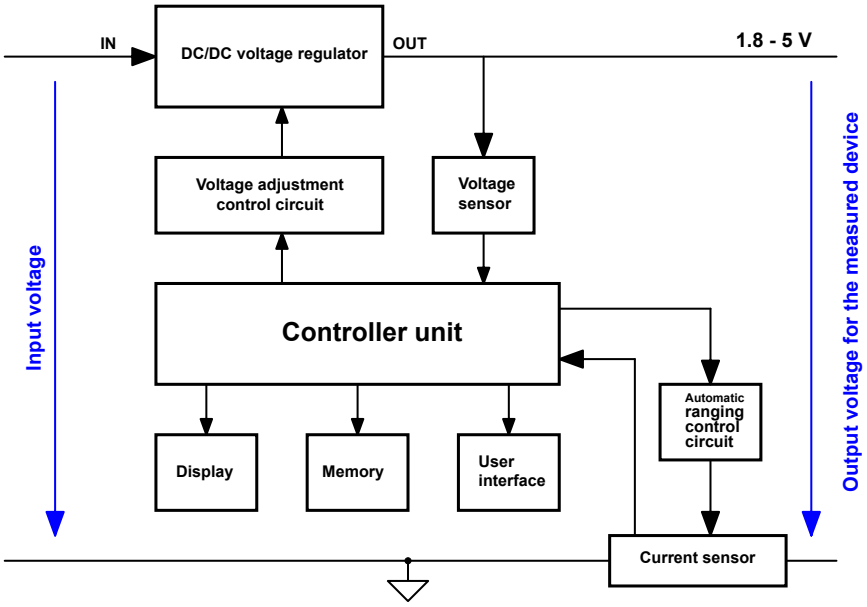

Figure 3.1: Block diagram

In the following list, each of the blocks is shortly introduced, the fundamental thoughts behind the design process are summarized, and the parameters that are not directly required by the assignment are further specified.

1. Regulator stage

   As the final product has to provide stable power to the measured device, while allowing output voltage adjustability, a regulator stage is necessary. However, the device is not to be designed to be powered from the wall AC power socket but counts with a presence of an external power brick or power supply. Thus a DC/DC voltage regulator is needed. Although the output voltage range is strictly set by the requirement, the input voltage is not. To allow convenience and ease of use, as the input voltage source, a USB connector is to be used, providing standardized $V_{IN} = 5\,\mathrm{V}$.

   In this stage, the protection of the output against short-circuit or over-current has to be considered. Instead of using complicated short-circuit

protection circuits, a voltage regulator with this function already integrated is to be used. Secondly, the currents that are not high enough to trigger the regulator's integrated over-current/short-circuit protection are to be detected by the onboard control unit, and the regulator shut down.

The theoretical background concerning voltage regulators and the ways of output voltage adjustment is previously discussed in section 2.4, while the actual design is described in section 3.3.

2. Current sensor

   The assignment requires an ability to measure very low currents with fast fluctuations to be expected. To specify, the device is to be designed to measure current as low as 1 µA and take samples at least once every 10 µs while still maintaining decent accuracy and precision.

   To achieve this, the only viable and cost-efficient method is to utilize a current sense resistor. For that purpose, a series of shunt resistors of different sizes are to be placed in the path of the current flow and switched between according to the amount of drawn current. They are to be followed by separate differential amplifiers and processed by a high-speed 16-bit analog-to-digital converter, which was available from previous projects.

   This method is implementable in either a low-side sensing or a high-side sensing variant. To mitigate a need for an external PMOS driver in the current switching method, low-side current sensing is to be selected. However, as the low-side current sensing may result in undesirable ground disturbance, a high-side current sensing should have been preferred. Nevertheless, the low-side is to be used, while a replacement for the high-side current sensor shall be subject to future project improvement.

   The theoretical background concerning current sensors and dynamic ranging is previously discussed in section 2.6 with analog-to-digital converter types and purposes introduced in 3.4.2. The actual design is described in section 3.4.2.

3. Output voltage sensor

   While a voltage reading is essential for the power consumption calculation, it is not expected to be nearly as fast-changing. The output voltage is expected to be nearly constant, with non-frequent output voltage adjustments being the exception. The constancy of the output voltage is also significantly affected by the regulator's stability and its load transient response.

   As the regulator is to be designed as low-noise and stable as possible, no external amplifiers and analog-to-digital converters are to be used to measure the output voltage. Instead, a simple voltage divider feeding a scaled-down signal to a less accurate ADC integrated into the control processing unit is to be used. The sensing wire is to be placed as close

to the regulator's output capacitor as possible. Due to this position, the voltage drop, hence the power loss, has to be accounted for during the power consumption calculation.

The design of the voltage sensor monitoring the output voltage is included in section 3.4.1.

4. Control unit

   To control the entire system, process, and transfer data from the sensors, a microcontroller is to be used. The main requirements for the microcontroller are high-speed (high operating clock frequency), the presence of ADC and DAC (with high enough resolution), and a sufficient amount of input and outputs. As the application requires data storage and transfer, a microcontroller with integrated FLASH memory and native USB protocol are to be used.

   While a theoretical introduction to microcontrollers and communication protocols is made previously in section 2.7, the selection and design itself are presented in section 3.5.

5. User interface

   To control the device and monitor the parameters without a computer connection, a design of a user interface is necessary. As one of the main functions that need to be controlled is the output voltage, two buttons are to be used, representing an increase, respectively decrease in the output voltage. Further functions may be implemented by utilizing long presses or double clicks.

   The measured and calculated data are to be displayed on an external display. While a cheaper LCD would suffice, due to direct availability, an OLED display was selected. An external display breakout board is to be used, interconnected with the designed printed circuit board via external wires, and housed with it in a custom enclosure.

   The design of the user interface is included in section 3.6.

After all of the previously described blocks are designed in their respective subsections, the last section of this chapter summarizes the device's capabilities and thermal properties (3.7).

3.3 Voltage regulator design

To successfully design an accurate and high-speed active power consumption meter, the foundation is a stable and reliable power source. For this project requirements were as follows:

- Output voltage - 1.8 - 5 V
- Output current - 0.5 A

On top of the requirements directly specified in the assignment, an input voltage of $V_{IN} = 5\,\text{V}$ was selected. The main purpose of this selection is to provide easy and convenient connectivity of the device. This way, the device can be powered by the most common power bricks (for example phone chargers) or directly via the computer's USB ports.

To achieve 1.8 - 5 V output voltage, a simple adjustable buck converter would seem like an ideal option. However, during testing, the switching regulator output noise in combination with only a decently accurate voltage sensor (3.4.1) has proved itself as a significant cause of power consumption measurement inaccuracies. To eliminate or at least suppress this issue, a decision to utilize a linear regulator was made. As discussed at the beginning of this paper (2.4.1), the linear regulator brings many advantages; however, introduces a significant voltage drop that would not allow 5 V output voltage with 5 V at the input of the regulator. For these reasons, a regulator chain consisting of a boost converter followed by a linear voltage regulator was designed and utilized.

The purpose of the boost converter is to increase the voltage level to approximately 5.5 V, leaving enough headroom for the second stage regulation. Moreover, as the boost converter is followed by the linear regulator, the precision, output noise, and other parameters are not as important, and the main concern was the price. For that reason, a low-cost boost converter LM2623 [65] was used, and the schematic was created 3.2.

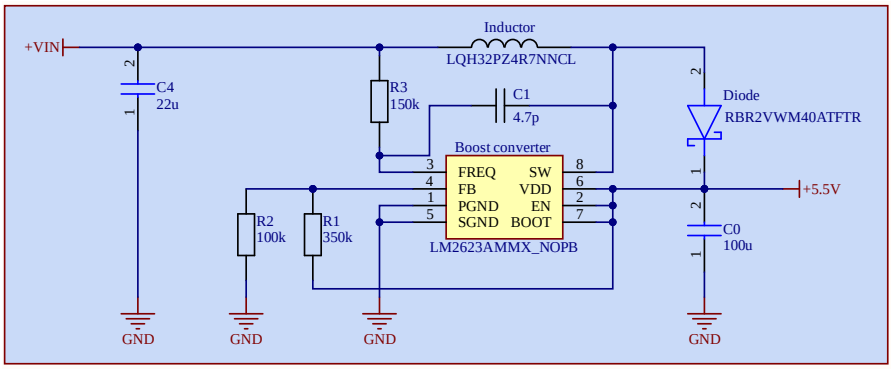

Figure 3.2: Schematic of the boost converter

Some of the most important features of the LM2623 boost converter are:

- 0.8 V to 14 V input voltage
- 1.24 V to 14 V output voltage
- adjustable switching frequency (300 kHz to 2 MHz)
- up to 2 A output current with built-in current limit
- up to 90 % efficiency

The selection of the individual passive components followed a guide described in the theoretical part of the paper 2.4.2. The feedback resistive network was then selected as:

$$R_1 = 340\,\text{k}\Omega \;; \qquad R_2 = 100\,\text{k}\Omega \tag{3.1}$$

Corresponding to an output voltage of:

$$V_{OUT} = V_{FB}\frac{R1 + R2}{R2} = 1.24 \cdot \frac{440}{100} = 5.456\,\text{V} \tag{3.2}$$

The required inductance of the inductor can be approximated as:

$$L = \frac{V_{IN} \cdot (V_{OUT} - V_{IN})}{\Delta I_L \cdot f_s \cdot V_{OUT}} \tag{3.3}$$

Substituting 1 MHz as the switching frequency f_s and 30 % of maximal expected output current (0.5 A) as ΔI_L, following value can be derived:

$$L = \frac{5 \cdot 0.456}{0.3 \cdot 0.5 \cdot 1 \cdot 10^6 \cdot 5.456} \sim 3\,\mu\text{H} \tag{3.4}$$

A standardized value of $L = 4.7\,\mu\text{H}$ was thus selected.

It must be noted that due to the output voltage being permanently set by the resistive network to $V_{OUT} = 5.456\,\text{V}$, a lot of pressure is put on the following linear regulator. This issue is further discussed in section 3.7, and a solution is proposed in the conclusion of the paper (5).

As power efficiency is not crucial for this application and better stability and low noise are much more essential, a low-dropout linear regulator was selected. Even though due to the simplicity of linear regulators, it would be possible to construct them using only common components (as shown in 2.4), the amount of available linear regulators is massive, and it is not hard to find one, that suits most of the applications. Moreover, commercially available regulators are thoroughly tested, optimized, and probably achieve much better stability and overall performance.

Even though TPS7A[66] (cheaper) was initially intended to be used, due to availability reasons, a relatively new integrated circuit LT1965IQ [67] from Analog devices was utilized. To ensure thermal stability even with a significant input-output voltage difference, a big DDPAK-5 package was selected. This LDO linear regulator offers:

- fast transient response, high precision, high PSRR, low-noise
- up to 1.1 A output current
- 1.2 V to 19.5 V output voltage
- up to 20 V input voltage

The designed schematic of the linear regulator is shown in figure 3.3, and the digital adjustability is discussed in section 3.3.1.

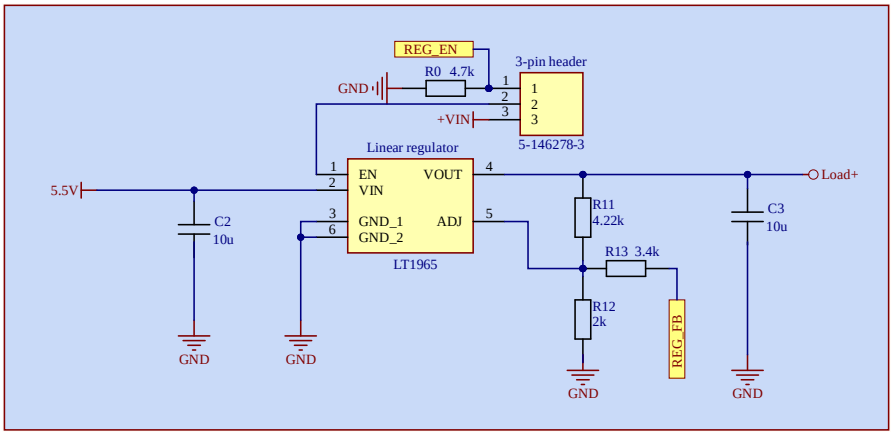

Figure 3.3: Schematic of the voltage regulator

3.3.1 Output voltage adjustability

By using an integrated circuit, an issue of digital adjustability of the voltage regulator's output voltage had to be managed. Thanks to the availability of external digital-to-analog signal from the utilized microcontroller (described later in the paper in section 3.5), the method 2.5.2 using a DAC signal to adjust the output voltage was implemented. This design can be observed in figure 3.3, where a resistor R_{13} with DAC output (pin REG_FB) is used. The 3-pin header is strictly for testing purposes, allowing to either tie the regulator's enable pin to the VIN (ON-state) or to a digital microcontroller output with a pull-down resistor.

To successfully adjust the voltage in the required range, a selection of resistors R_{11}, R_{12} and R_{13} had to be made. To choose the correct values, the following equations can be derived:

$$R_{12} = V_{FB} \cdot R_{11} \cdot \frac{(V_{DACH} - V_{DACL})}{\begin{array}{r} V_{FB} \cdot (V_{OUTL} - V_{OUTH} + V_{DACL} - V_{DACH}) \\ -(V_{DACL} \cdot V_{OUTL}) + (V_{DACH} \cdot V_{OUTH}) \end{array}} \tag{3.5}$$

$$R_{13} = R_{11} \cdot R_{12} \cdot \frac{(V_{DACH} - V_{FB})}{(R_{12} \cdot V_{FB)} + (R_{11} \cdot V_{FB}) - (R_{12} \cdot V_{OUTL})} \tag{3.6}$$

where:

V_{FB} is the feedback voltage – can be found in the datasheet
V_{DACH} is the maximal DAC output voltage
V_{DACL} is the minimal DAC output voltage
V_{OUTL} is the minimal required output voltage
V_{OUTH} is the maximal required output voltage

Using equations 3.5 and 3.6 and these predetermined parameters (some values were selected a little bit higher or lower than required to leave a little bit of space for adjustment caused by inaccuracies):

$$\begin{aligned} V_{FB} &= 1.24\,\mathrm{V}\ ; \quad & V_{DACH} &= 3.0\,\mathrm{V}\ ; \quad & V_{DACL} &= 0\,\mathrm{V} \\ R_{11} &= 30\,\mathrm{k\Omega}\ ; \quad & V_{OUTH} &= 5.2\,\mathrm{V}\ ; \quad & V_{OUTH} &= 1.5\,\mathrm{V} \end{aligned} \tag{3.7}$$

desired resistor values can be calculated. The values of the resistors were intentionally selected relatively low to ensure the stability of the regulator. After rounding up the values to the closest commercially available value, the following resistors were chosen:

$$R_{11} = 4.22\,\mathrm{k\Omega}\ ; \quad R_{12} = 2\,\mathrm{k\Omega}\ ; \quad R_{13} = 3.4\,\mathrm{k\Omega} \tag{3.8}$$

The output voltage can then be calculated as 3.9, and the dependence is plotted in figure 3.4.

$$V_{OUT} = (1 + \frac{R_{11}}{R_{12}}) - \frac{R_{11}}{R_{13}} \cdot (V_{DAC} - V_{FB}) \tag{3.9}$$

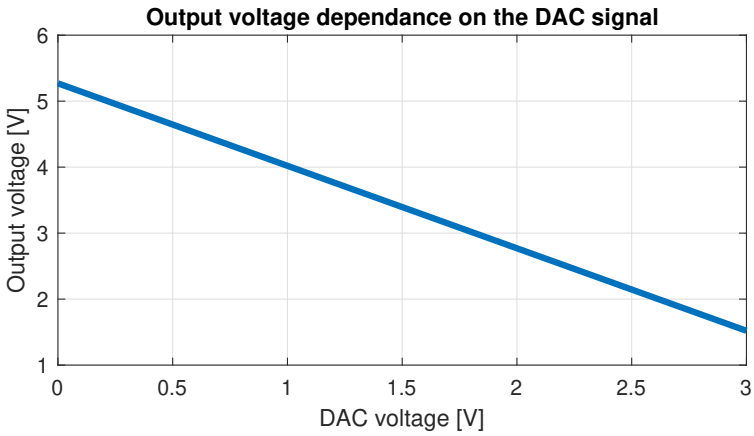

Figure 3.4: Calculated output voltage dependence on the DAC signal

The graph 3.4 shows that the resistor value calculations were correct, featuring an output voltage of 1.52 V to 5.27 V. Considering an 8-bit DAC with 3.3 V reference, a step size of 0.0148 V was calculated.

3.4 Power consumption meter design

Even though a current and voltage reading is needed for a power consumption calculation, this section primarily focuses on the design of a current sensor. When the voltage regulator is well designed, the voltage readings should be more stable, thus requiring less precise measurements.

3.4.1 Voltage sensor design

To measure the output voltage, a simple voltage divider was utilized, dividing the output voltage to a level acceptable by the AD converter.

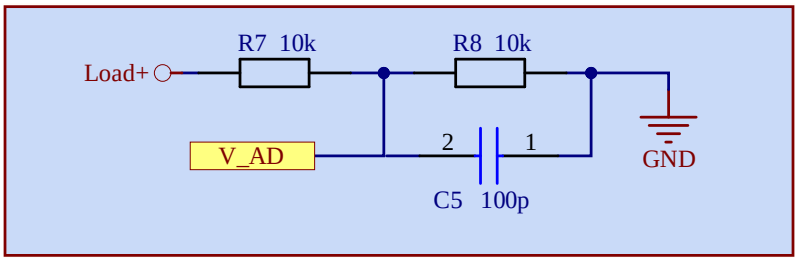

Figure 3.5: Schematic of output voltage measurement circuit

A 1:1 division ratio was selected (as shown in 3.5). A simple equation can be derived as:

$$V_{LOAD+} = V_{V\_AD} \cdot \frac{R7 + R8}{R8} = 2 \cdot V_{V\_AD} \tag{3.10}$$

Pin V_AD is connected to the internal ADC of the utilized microcontroller, allowing a 12-bit reading with a sampling rate of 200 ksps. Considering a 3.3 V ADC reference voltage, an output voltage of 0 V up to 6.6 V can be measured with an ideal resolution of:

$$\text{V\_AD}_{res} = \frac{3.3}{2^{12}} \sim 800\,\mu\text{V} \tag{3.11}$$

However, it shall be noted that the sufficiency of the sampling speed and accuracy is highly dependent on the stability of the voltage regulator.

To improve the accuracy of the measurement, a capacitor $C5$ was placed parallel to resistor $R8$. Because of the relatively high sampling frequency and the fact that the voltage divider and the capacitor $C5$ combined with ADC sampling capacitance form a simple RC filter, the cut-off frequency must be checked.

$$f_c = \frac{1}{2\pi \cdot R \cdot C_{IN}} \tag{3.12}$$

The cut-off frequency can be calculated using equation 3.12, where C_{IN} is the input capacitance ($C5 + C_{SAMPLE}$) and R is a parallel combination of $R7$ and $R8$. According to the datasheet [55], the sampling capacitance (C_{SAMPLE}) is around 2 pF. When the values are substituted to equation 3.12, the following value can be derived:

$$f_c = \frac{1}{2\pi \cdot 5000 \cdot (2 \cdot 10^{-12} + 100 \cdot 10^{-12})} \sim 317\,\text{kHz} \tag{3.13}$$

Considering the sampling rate, this value satisfies the requirement.

3.4.2 Current sensor design

In contrast to the voltage measurement, current readings tend to fluctuate much more and require more attention. As stated at the beginning of the paper, the assignment requires a fast and accurate current sensor to measure small current fluctuations (units to tens of µA) with short current pulses (tens of µs). Measurements with these parameters should be achieved over a wide dynamic range of 0 - 0.5 A.

Current shunt switching circuit

From the available current sensing options (2.6), only the Ohm's based methods and logarithmic amplifier arise as valid solutions for these requirements. However, achieving such accuracy with a logarithmic amplifier would be nearly impossible, thus making the Ohm's based methods the most suitable current sensing technique for this application. To achieve a compact and integrated design, the surface-mounted shunt resistor (2.6.1) is utilized.

Nevertheless, not even a single shunt resistor was sufficient to achieve the needed accuracy over such a wide dynamic range. This issue is demonstrated in the second chapter in section 2.6.5. A current shunt-switching technique is thus utilized (2.6.5) and shown in figure 3.6.

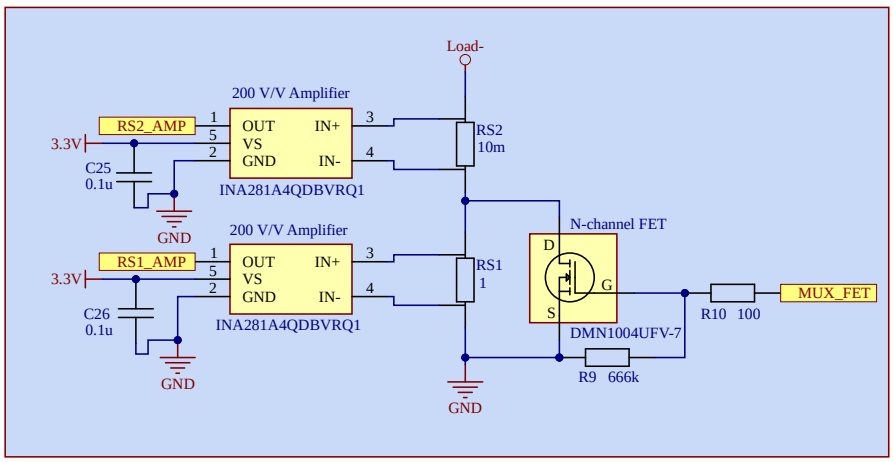

Figure 3.6: Schematic of shunt switching circuit

An important step in the design is a selection of a current range, which each individual current shunt resistor is going to process. From previous research, most of the microcontrollers, while idle or under light load, consumed under 10 mA of current.
For this purpose, the maximal measurable current on the bigger shunt resistor was selected as:

$$I_B = 15\,\text{mA} \tag{3.14}$$

When the current I_B or larger is detected, the MOSFET parallel to R_{S1} is to be turned on and thus creating a low-resistance path for the current. In

this scenario, signal $RS2\_AMP$ is to be processed by the ADC. For currents smaller than I_B, resistor R_{S1} is to be active with signal $RS1\_AMP$ being processed.

The schematic 3.6 shows two shunt resistors with different resistance. To improve DC, as well as high-frequency performance, bulky, low-inductance current sense resistors were used. The selected types, values, and key parameters are featured in the following table 3.1.

Resistor	**RS1**	**RS2**
Value	1 Ω	0.01 Ω
Type	ERJ-12ZQF1R0U	LVK25R010CER
Tolerance	1%	0.25 %
TCR	100ppm	100ppm
Termination	2 Terminal	4 Terminal
Case code - in	2010	2412

Table 3.1: Current shunt resistors key features

Even though power efficiency is not crucial in the regulator stage, these values were selected low enough so the caused power loss is not too large and thus as much power as possible is available for the load, respectively the connected measured device. Furthermore, the values are strategically chosen so both amplifiers may be chosen with the same gain and still satisfy the input range of the utilized ADC.

A standardized amplifier gain value that allows utilizing a majority of the ADC's input range with previously stated current shunt resistors (3.1) and the border current I_B (3.14) is 200. For these reasons, the INA281A4 [69] amplifiers were placed after each shunt resistor providing a high gain of 200 V/V with high bandwidth of 1.3 MHz. The usage of two separate amplifiers can be justified by a need for differential inputs utilizing the Kelvin connection.

Differential amplifier	**INA281A4**
Gain	200 V/V
Gain error	TYP ± 0.07 %
Bandwidth	900 kHz[a]
Slew rate	2.5 V/µs
Offset voltage	TYP ± 55 µV
CMRR	120 dB [b]; 65 dB [c]

[a] $C_{LOAD} = 5\,\text{pF}; V_{SENCE} = 20\,\text{mV}$

[b] DC CMRR ; [c] AC CMRR at 50 kHz

Table 3.2: INA281A4 key features

When choosing the switch parallel to R_{S1} (in this case, an N-channel MOSFET), a great deal of emphasis has to be placed on the $R_{DS(ON)}$ parameter. This is because choosing a MOSFET with $R_{DS(ON)}$ as low as possible ensures

minimal power losses when the MOSFET is turned on. For that purpose, a DMN1004UFV-7 [68] from DIODE incorporated was selected, showing only around 4 mΩ of on-state resistance. On top of that, the MOSFET supports 3 V logic and thus can be operated using a digital signal of a microcontroller.

N-channel MOSFET	DMN1004UFV-7
Drain-Source ON-resistance	$\sim 4\,\mathrm{m\Omega}$ [a]
Maximal drain current	$\sim 60\,\mathrm{A}$ [a]
Gate Threshold Voltage	MAX 1 V
Turn-On Rise Time	10.8 ns [b]
Turn-Off Fall Time	16.9 ns [b]

[a] $V_{GS} = 3.3\,\mathrm{V}$

[b] $V_{DS} = 6\,\mathrm{V}$; $V_{GS} = 4.5\,\mathrm{V}$;$R_G = 1\,\Omega$; $I_D = 5\,\mathrm{A}$

Table 3.3: DMN1004UFV-7 key features

Signal multiplexer

The output signal from each of the amplifiers is then routed to a simple 1-bit analog multiplexer TS5A2053DCTR [70].

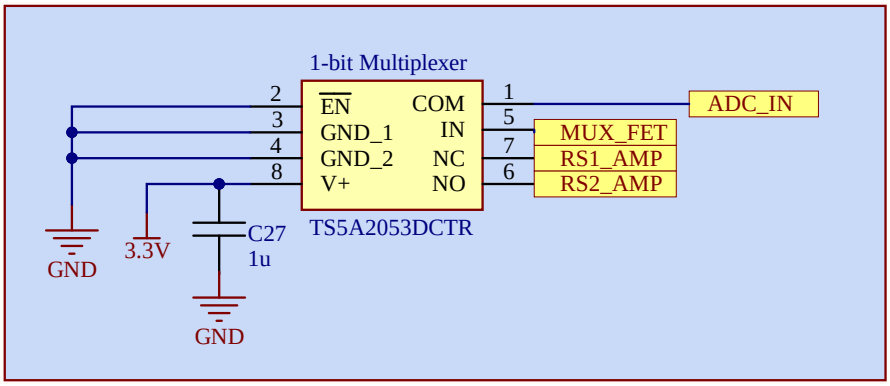

Figure 3.7: Schematic of multiplexer connection

The reasoning behind this design, instead of directly utilizing multi-channel ADC, is that no multi-channel ADC with high enough resolution and sampling rate was available. In addition, the use of two separate ADC would significantly increase the cost, and since there is never required to conduct a measurement simultaneously on both shunt resistors, a signal multiplexer was the best choice.

Analog-to-digital converter sampling

The signal from the multiplexer is then fed to an external analog-to-digital converter. While choosing the analog-to-digital converter, multiple options with different parameters and suitable for different applications arise (described in section). Two parameters were essential for this application:

1. sufficient sampling speed

2. sample resolution

To allow the detection of fast current spikes, a sampling rate of 1 Msps was chosen. Due to previous experiments, a successive-approximation MCP33131-10 [71] analog-to-digital converter from Microchip Technology with this sampling rate was available. On top of that, it features a 16-bit resolution, which shall be more than sufficient for this application. Some fundamental parameters of the ADC are shown in table 3.4.

Analog-to-digital converter	**MCP33131-10**
Type	Successive-approximation
Sampling frequency	1 Msps
Resolution	16-bit
Offset error	± 0.1 mV
Gain error	± 4 LSB
Signal-to-Noise Ratio	86.7 dBFS
Integral Nonlinearity	± 2.2 LSB
Differential Nonlinearity	± 0.9 LSB

[a] $V_{REF} = 5\,\text{V}; f_{IN} = 10\,\text{kHz}$

Table 3.4: MCP33131-10 key features

Even though the MCP33131-10 supports a 3.3 V reference voltage, it also requires a 1.8 V analog supply voltage; thus, a secondary voltage regulator is needed. For that purpose, a TPS73118 [72] LDO regulator was utilized, creating a 1.8 V from the available 3.3 V. This part of the circuit is shown in 3.8.

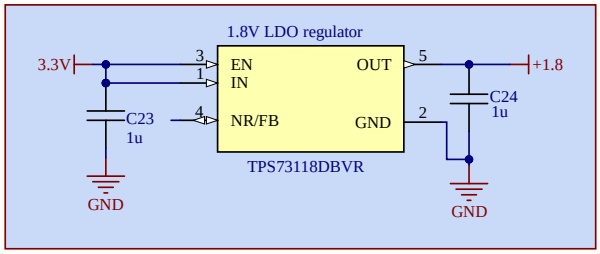

Figure 3.8: Schematic of 1.8 V supply for ADC

Finally, a schematic of the analog-to-digital converter itself was created 3.9. The schematic shows not only the ADC itself but also individual control and data signals connected to it. An output of the multiplexer (*ADC_IN*), as well as the SPI data signal (*ADC_SDO*) with its control signals (*ADC_CNVST*, *ADC_SCLK*) are present.

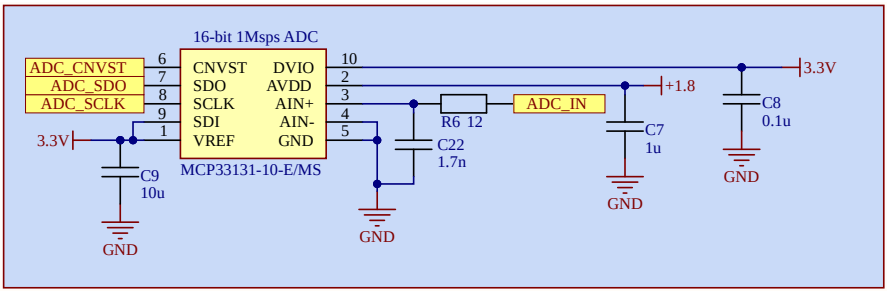

Figure 3.9: Schematic of the utilized ADC

With this ADC and the amplifiers described in section 3.4.2, the smallest measurable voltage can be derived as:

$$ADC_{LSB} = \frac{V_{ADCref}}{ADC_{res}} \cdot \frac{1}{G} = \frac{3.3}{2^{16}} \cdot \frac{1}{200} \sim 251\,\text{nV} \tag{3.15}$$

This value is considerably lower than the offset voltage of the utilized amplifiers and thus the lower bits of the information would become invalid, hence an offset compensation is needed. However, since the data are processed by a microcontroller, this issue is resolved in the software part of the device, where the offset was compensated for the specific piece of the INA281A4 amplifier.

To further improve the current readings, a simple anti-aliasing low-pass filter is placed at the input of the ADC. To select the RC filter values, someone may consider simply selecting a value satisfying the Nyquist sampling theorem. However, too much band-limiting will increase the settling time and distort the input signal [73].
To calculate the value, the following procedure was followed. Firstly, a maximum amplifier output change was selected as $V_{CH} = 3\,V$ (current through R_{S1} jumping from 0 mA to 15 mA. With this value, the input sampling capacitance C_{INT} (found in the datasheet) and the selected RC filter capacitance C_{EXT}, an equation 3.16 describing the step size, that needs to be settled, was derived.

$$V_{STEP} = \frac{V_{CH}C_{INT}}{C_{EXT} + C_{INT}} = \frac{3\,\text{V} \cdot 31\,\text{pF}}{1.7\,\text{nF} + 31\,\text{pF}} = 53.72\,\text{mV} \tag{3.16}$$

With the value calculated in 3.16, a number of time constants necessary to settle $\frac{1}{2}$ LSB was calculated.

$$N_\tau = \ln\left(V_{STEP} \cdot \frac{2^{ADC_{bit}+1}}{V_{ADCref}}\right) = \ln\left(35.82\,\text{mV} \cdot \frac{2^{16+1}}{3.3\,\text{V}}\right) = 7.67 \tag{3.17}$$

where ADC_{bit} refers to the bit resolution and V_{ADCref} specifies a voltage reference of the analog-to-digital converter. Finally, the required time constant can be derived as:

$$\tau_{RC} = (t_{SR} - t_{CONV}) \cdot \frac{1}{N_\tau} = \left(\frac{1}{1\,\mathrm{Ms\,s^{-1}}} - 700\,\mathrm{ns}\right) \cdot \frac{1}{7.67} = 39.13\,\mathrm{ns} \quad (3.18)$$

where t_{SR} is equal to an inverse value of an ADC's sampling rate and t_{CONV} is the data conversion time. The equivalent bandwidth of the low-pass RC filter is then

$$BW_{RC} = \frac{1}{2\pi\tau_{RC}} = 4.06\,\mathrm{MHz} \quad (3.19)$$

resulting in a resistor value of 24 Ω. Including the 10 Ω resistance of the utilized multiplexer, a value of $R_6 = 12\,\Omega$ was selected. This procedure was highly inspired by an article distributed by Analog Devices [73]. However, due to the lack of computing power and inability to utilize the full 1 Msps sampling frequency in the final design, the values of the actual RC filter present on the PCB were later adjusted and fine-tuned.

Capabilities

This entire shunt-switching design was constructed to improve accuracy without too much additional power loss. However, to fully utilize the design, a correct boundary when the shunts are switched has to be chosen. Furthermore, properties have to be defined and resolution capabilities calculated to substantiate this design choice.

The selected boundary value, when the MOSFET 3.4.2 is switched on, was selected as:

$$I_B = 15\,\mathrm{mA} \quad (3.20)$$

An overview of parameters and properties is demonstrated in table 3.5.

Shunt Resistor	$\mathbf{R_{S1}}$	$\mathbf{R_{S2}}$
Value	1 Ω	10 mΩ
Current range	0 - 15 mA	15 mA - 1 A
Maximal power loss	0.225 mW	10 mW
Maximal amplifier output	3 V	2 V

Table 3.5: Shunt resistor capabilities

Moreover, when the resistor R_{S1} is bridged by the utilized MOSFET, an additional maximum power loss of $\sim 5\,\mathrm{mW}$ can be expected.

The ideal current resolution using the shunt resistor R_{S1} and not including offsets, thermal drifts, and other inaccuracies can be calculated as:

$$I_{RS1res} = \frac{V_{ADCref}}{ADC_{res}} \cdot \frac{1}{G} \cdot \frac{1}{R_{S1}} = \frac{3.3}{2^{16}} \cdot \frac{1}{200} \cdot \frac{1}{1} \sim 251.112\,\mathrm{nA} \quad (3.21)$$

The same principle applies for the second shunt resistor R_{S2}.

$$I_{RS2res} = \frac{V_{ADCref}}{ADC_{res}} \cdot \frac{1}{G} \cdot \frac{1}{R_{S2}} \sim 25.177\,\mu\mathrm{A} \quad (3.22)$$

3.5 Control circuit design

As the control circuit of the entire circuit, the EPS32-S2 [55] SoC from Espressif Systems was selected. The main reasoning behind this choice is the available support from the school, and active online support team, as well as the fact, that Espressif Systems have offices in the Czech Republic, and getting to know the ESP architecture may be beneficial for my future.

Furthermore, this microcontroller comes not only in a single compact package but is present on many prefabricated breakout boards. In addition, it comes with many important interfaces and features, while the essential ones are listed below:

- low-power SoC microcontroller solution
- up to 240 MHz operating frequency
- 4 MB of Flash memory
- 12-bit analog-to-digital converter
- 8-bit digital-to-analog converter
- communication interfaces - UART, USB, I2C, I2S, SPI
- enough input and output pins

On top of the features listed above that were in some way essential to the design, the ESP32-S2 microcontroller provides various options for wireless data transfer. This includes a simple Bluetooth interface but also a Wi-Fi, fully compliant with the IEEE 802.11b/g/n protocol [55]. Even though these features were not utilized, they are a nice addition to an already powerful chip that could enable IoT integration in future project revisions.

To simplify the design and eliminate the need to hand solder a 56-pin QFN package, an open-source development board Adafruit QT Py was utilized. Firstly, not only is the desired ESP32-S2 microcontroller present, but the compact footprint of the board allows for a high-level integration with all the necessary circuitry required for the microcontroller operation already included. Secondly, the board provides multiple GPIO pins, including all the necessary communication interfaces (I2C – with universal STEMMA connector, SPI, UART, and others). Lastly, the board provides a USB-C connector, which can be used for communication with a computer, programming, and debugging but can also serve as the voltage source for the power consumption meter's voltage regulator (this is further specified in section 3.7).

These features can be easily accessed and re-programmed using higher-level programming languages like Python or C++ with numerous open-source libraries, thus providing much simpler solutions for design development.

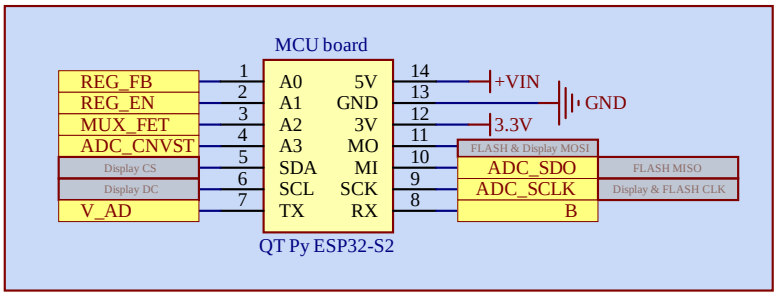

Figure 3.10: Schematic of the control circuit

The schematic showing the ESP32-S2 board connected to the rest of the circuitry is included in figure 3.10. The ports represented with yellow background symbolize an actual PCB trace connection, and their respective counterparts are present in the individual schematics included in previous sections. On the other hand, ports represented in grey symbolize hard-wired connections using 24 AVG wire between the microcontroller board at the OLED display (3.6.1).

3.6 User interface design

Even though the device provides superior system communication and the required control buttons and the measured data could be implemented in a computer application, a user interface was implemented to provide a computerless control option. The design uses a set of buttons with a display to adjust the output voltage and provide real-time monitoring.

3.6.1 Display

A large enough display had to be selected to provide enough space for all the necessary readings, including current power consumption, average power consumption, output voltage, and other data. For this reason, a 1.5 inch OLED display was selected. Specifically, Adafruit Grayscale 1.5" 128x128 OLED Display [78].

Not only does this provide a large display area for all the data, but it also offers an option to utilize an SPI interface instead of the usually present I^2C connection. This may not seem important, but for applications requiring fast computing, the speed advantage of SPI interface is noticeable and thus more suitable.

3.6.2 Buttons

The voltage output adjustment and other control commands are taken care of by two external buttons. However, the utilized Qt PY board 3.5 does not accessibly provide all the microcontroller pins, thus making it impossible to use two digital pins as the button inputs. Because of that, a solution using only one analog microcontroller input was designed 3.11

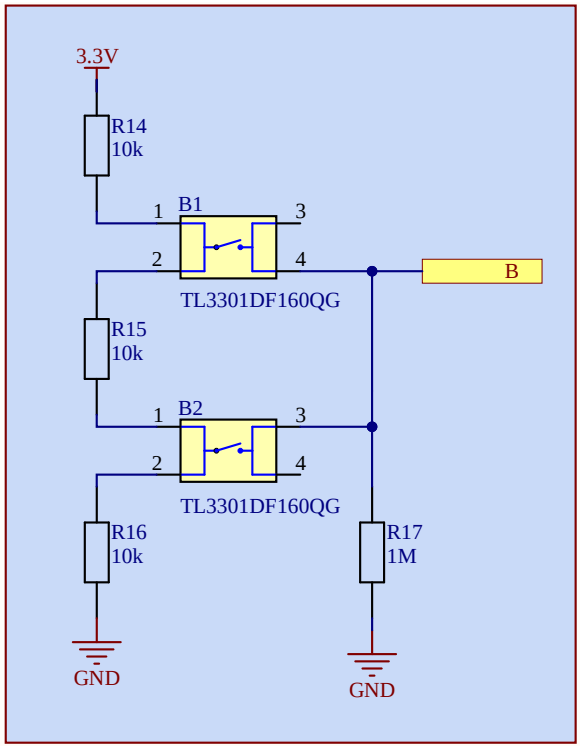

Figure 3.11: Schematic of the two buttons utilizing one analog input

This solution utilized the basic principle of voltage divider bridged by the respective buttons. Utilizing this design allows for a single microcontroller analog input to be used instead of two digital inputs.

When no button is pressed, there is 0 V on the B pin thanks to the R_{17} pull-down resistor. However, when button B_1 is pressed a voltage divider is formed between resistor R_{14} and resistors $R_{15} + R_{16}$ creating a 1:2 ratio. This results in a voltage of:

$$V_B = V_{IN} \cdot \frac{R_{15} + R_{16}}{R_{14} + R_{15} + R_{16}} = 3.3 \cdot \frac{200 \cdot 10^3}{300 \cdot 10^3} \sim 2.2\,\text{V} \tag{3.23}$$

The same principle applies when B_2 is pressed, however the resistor ratio changes to 2:1 with a readable voltage of:

$$V_B = V_{IN} \cdot \frac{R_{16}}{R_{14} + R_{15} + R_{16}} = 1.1 \cdot \frac{100 \cdot 10^3}{300 \cdot 10^3} \sim 1.1\,\text{V} \tag{3.24}$$

Pressing both buttons at the same time creates a low-resistance path over R_{15}, achieving a 1:1 ratio between R_{14} and R_{16}.

3.7 Output capabilities

In the last section of this chapter, the output capabilities of the designed system are discussed and concluded. As far as the maximum output current

capabilities are concerned, there are many factors and components that directly affect it.

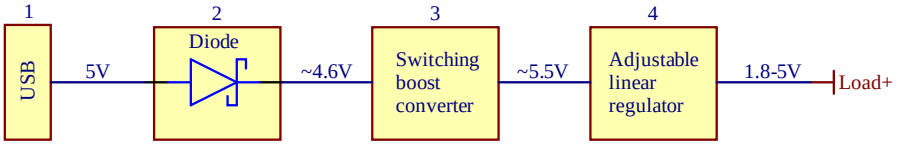

Figure 3.12: Schematic of the voltage supply management

The sequence starting from the input source – USB, up to the adjustable output voltage is shown in figure 3.12. Each section brings its own limitations and restrictions, which are shortly described in the list below.

1. USB connection
   - considering the nowadays standardized USB 3.0 connection, the maximal power provided is 4.5 W, which translates to 900 mA and 5 V
2. USB protective diode
   - the utilized QT Py board, which includes the USB-C connector, also comes with a NSR102 Schottky diode protecting the host computer USB ports
   - the diode allows maximal forward current of 1 A, while at that point requiring around 0.45 V forward voltage.
3. Switching boost converter
   - up to 2 A load current, around 87 % efficiency with $I_L = 0.9\,\text{A}$ and $V_{OUT} - V_{IN} \sim 1\,\text{V}$
4. Adjustable linear regulator
   - linear regulator with significant power loss, the maximal output current of 1.1 A and dropout voltage around 300 mV under maximum load
   - by the nature of linear regulators, the output current is essentially identical to the input current

Considering all the above-mentioned factors, the following equation for the maximal output current can be derived:

$$I_{OUTmax} \sim \frac{(V_{IN} - V_{FW}) \cdot I_{IN}}{V_{boostOUT}} \cdot V_{boostEFF} \tag{3.25}$$

where:

V_{IN} is the input voltage – USB level
V_{FW} is the forward voltage of the protective diode
I_{INmax} is the maximum input current
$V_{boostOUT}$ is the output voltage of the utilized boost converter
$V_{boostEFF}$ is the efficiency of the utilized boost converter

After substitution of the values from 3.7 to equation 3.25 following value can be calculated:

$$I_{OUTmax} \sim \frac{(5 - 0.45) \cdot 0.9}{5.5} \cdot 0.87 = 0.647\,\text{A} \tag{3.26}$$

To provide some headroom, leave enough energy for the microcontroller and other external circuitry, and not to push the components to their limits, the current which was in the software part evaluated as the maximum current was set to $I_{OUTmax} = 0.5\,\text{A}$. The final output capabilities are:

	Parameter
Output voltage	1.8–5 V
Maximal output current [a]	500 mA

[a] Refers to a continuous current draw

Table 3.6: Supply and output voltage capabilities

However, as the utilized voltage regulator is a linear regulator, the difference between input and output voltages plays a huge role in the device's capabilities. The LT1965 in the DD-PACK package offers a maximum junction temperature of 150 °C with a thermal resistance of around 30°C/W. Considering the following parameters and omitting the ground pin current:

$$I_{OUT} = 500\,\text{mA}$$
$$V_{IN} = 5.5\,\text{V}$$
$$V_{OUT} = 1.8\,\text{V}$$
$$T_{AMB} = 40°\text{C}$$

a junction temperature can be calculated as:

$$\begin{aligned} T_J &= T_{\text{AMB}} + (V_{IN} - V_{OUT}) I_{OUT} R_T \\ &= 40°\text{C} + (5.5\,\text{V} - 1.8\,\text{V}) \cdot 0.5\,\text{A} \cdot 30°\text{C/W} = 95.5°\text{C} \end{aligned} \tag{3.27}$$

While not ideal, the junction temperature is well below the maximum values the regulator can handle. The significant input-output difference is the reason the bulky DD-PAK package was necessary. This means that while on the

lowest 1.8 V output voltage setting, the regulator may become hot (however not terminally), the more commonly needed voltages like 3.3 V or 5 V will not result in a significant temperature increase. To completely eliminate this, instead of the boost converter, a buck-boost converter could be used and its output voltage adjusted by the same DAC signal as the linear regulator; however, with some voltage overhead greater than the LDO's dropout voltage.

Chapter 4

Implementation and measurements

4.1 Circuit implementation

Based on the previous chapter and the partial circuit schematics, a final circuit design was created. As a voltage regulator, an LT1965 was used (3.3) with its output voltage measured using a voltage divider (3.4.1) and integrated microcontroller ADC. The output current was measured using the shunt switching method (3.4.2), followed by a multiplexer (3.4.2) and a 16-bit 1 Msps analog-to-digital converter (3.4.2). The entire circuit is then controlled by an ESP32-S2 SoC (3.5). As a part of the design, an SPI display was used (3.6.1) with two external buttons (3.6.2), giving the user the ability to control the circuit without a need for a computer.

The complete schematics with respective resistor and capacitor values are shown in the attachment section (6.1).

4.2 Printed circuit board implementation

As said in the previous chapter in section 3.5, the device consists of two separate printed circuit boards that are interconnected together. While designing the printed circuit board, an effort was made to minimize the board size. However, all the component choices, as well as the spacings between components, were designed, so an assembly using a hand-held soldering iron is possible. Moreover, a great deal of emphasis was placed on correct layout techniques, including Kelvin connection, impedance matching, or separation of analog and digital grounds.

To help visualize the assembled board and allow an easy design of the enclosure and other attachments, a 3D model of the board was constructed. While some of the 3D models were purpose-built from the ground up, others were obtained through online libraries like `SnapEda.com` or directly from the component distributors like `Mouser.com`.

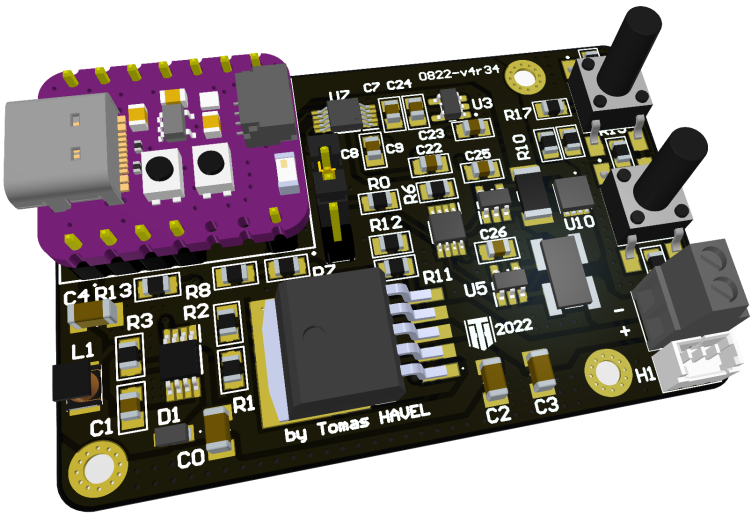

Figure 4.1: Printed circuit board 3D model

As seen in the model 4.1, by saving a significant amount of horizontal space by utilizing the ESP32-S2 QT Py board, the linear regulator's package could have been selected larger and thus improving the thermal capabilities of the device.

Lastly, the printed circuit board size and hole positions were explicitly designed to fit most of 1.5 inch OLED displays on top of the board. Also, the buttons are strategically placed so as not to be obstructed by the potential display. All the respective design files (PCB layers, circuit schematic) are included in the attachment section – 6.1,6.2,6.3.

4.2.1 Final PCB design and connectivity

The printed circuit board was then manufactured, and the respective components were assembled. The fully assembled board (front side and back side) is presented in 4.2, while a ruler in centimeters is included to visualize the actual size of the PCB.

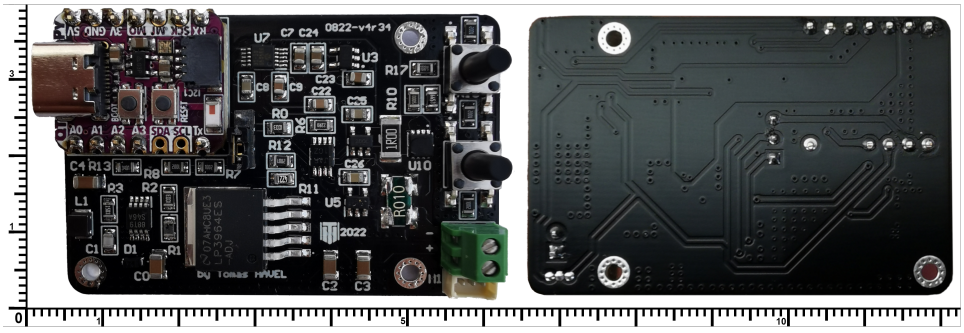

Figure 4.2: Front and back side of the implemented PCB

Since the board itself has multiple connection points, the following figure describes the purpose of individual connections.

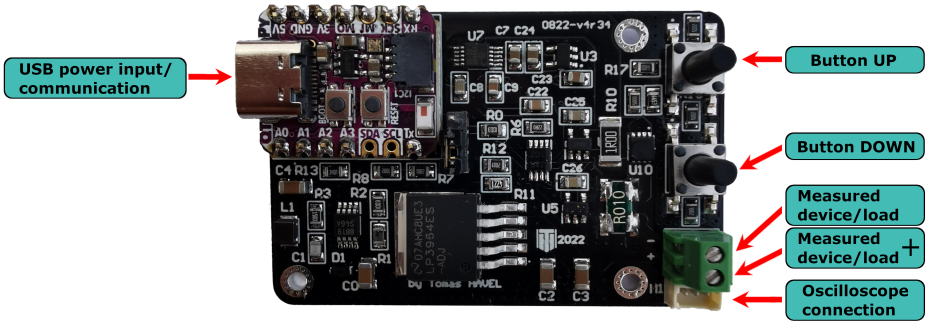

Figure 4.3: PCB connectivity

The oscilloscope connector is further explained in section 4.6.1.

4.3 Enclosure

As mentioned before, the completed device does not only consists of the printed circuit board but also includes an external display. Therefore, to house the circuitry and the display but also provide accessible connection points and buttons, a 3D model of an enclosure for the device was modeled. The enclosure was then 3D printed using MJF Nylon 12, providing sufficient strength, durability, and thermal endurance.

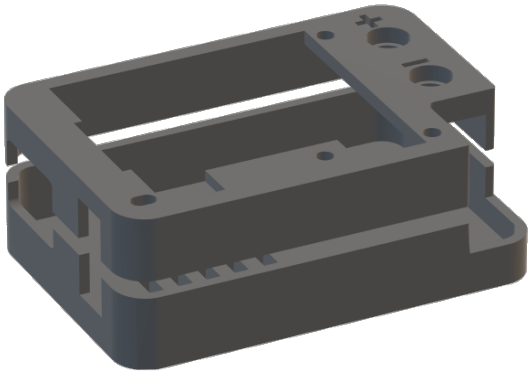

Figure 4.4: 3D model of the designed enclosure

The enclosure utilizes two separate parts with three holes in each part, allowing for a simple interconnection using bolts and nuts.

4.4 Final device

A picture of the final device utilized for the following measurements and tests is shown in 4.5.

Figure 4.5: Completed device

Thanks to its very compact size and ability to be powered directly from the computer's USB port, the device is an ideal alternative, if the embedded design engineer tends to move between places and bringing an oscilloscope, voltmeter, and bulky power supply is not an option.

4.5 Software implementation

To provide the control and adjustability functions, as well as the ability to precisely monitor the measured data, a software implementation is required.

The software was divided into two main sections. The first part, programmed into the integrated microcontroller, takes care of all the measurements and onboard control and provides superior system communication.

At the other end, specifically using a custom computer application, the provided data are captured, processed, and displayed. Moreover, direct control over the device's behavior (output voltage, enable) is supported via the application.

4.5.1 Device software

In the following figure 4.6, the development diagram is presented. Even though the diagram shows mainly the device's program side, the computer control is also present in the diagram.

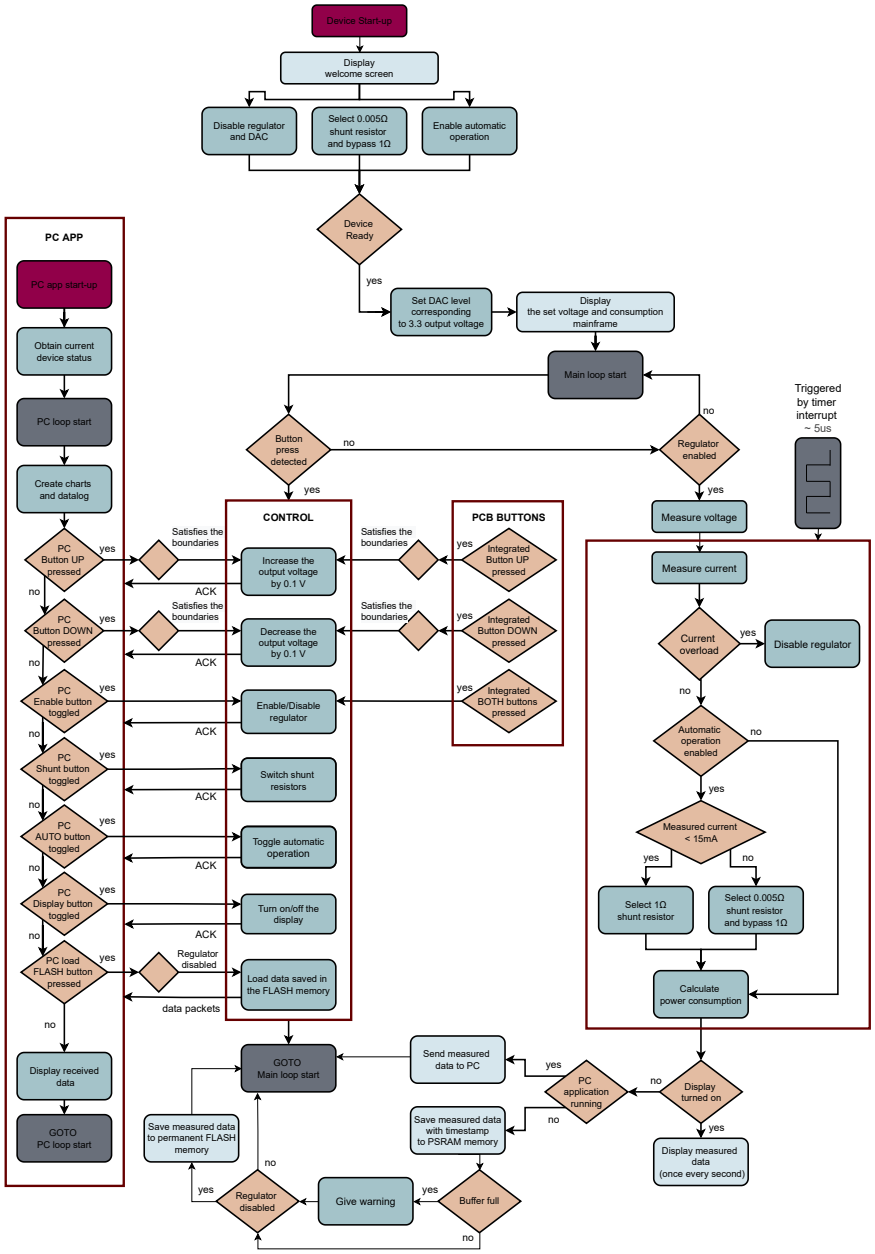

Figure 4.6: Software implementation diagram

To briefly summarize the program, when the device is connected via the USB port, a welcome screen is first shown. During the welcome screen, the device is prepared for operation (DAC set, current sensor prepared). When the device is ready, a screen showing all the monitored units and parameters is displayed. The regulator is disabled and awaits the user to manually turn it on – via the application or integrated buttons. When turned on, the main loop is entered. In the loop, the current and voltage measurements are taken, while the status of integrated and PC buttons are continuously checked. These buttons

control the adjustment and enable or disable the regulator but can also toggle automatic operation. When enabled, the device automatically switches between the two shunt resistors based on the current readings. During the automatic operation, when a current over 0.5 A is detected, the regulator is disabled, and manual re-enable is required. However, this function can be disabled in the computer app, giving the option to control the shunt selection manually. It shall be noted that no overload protection is active with the automatic operation disabled.

The power consumption, with its average, minimal and maximal values, is then calculated and displayed on display. When calculating these values, the power loss caused by the elements in the current's path (resistors, switch) is considered, and the values are accordingly adjusted. Finally, the data are then either sent via USB to the computer and displayed in the application (when the application is running) or momentarily stored in PSRAM memory. After the measurements are completed and the regulator thus disabled, measured data are moved from PSRAM to permanent FLASH memory. After this step, the entire loop is repeated.

Due to the sheer amount of data processing, serious attention had to be paid to final program optimization. To provide faster power consumption readings, the data are sent via the USB only when the application is running. Moreover, an option to turn off the display is present, eliminating the time required to display the data. Even though the presented diagram 4.6 implies one continuous uninterrupted loop, for crucial measurements (current readings) an interrupt handler was utilized. This ensures that the measurements are taken consistently at each preprogrammed time, while the functions with lower priorities (display refresh) are in the main loop and are processed when no interruption is being handled.

The diagram 4.6 is by no means the entire program with all the functionalities shown; however, it shall introduce the thought process behind the software implementation.

4.5.2 Communication protocol

To provide an easy way to monitor the data and control the device, a computer application was programmed. Before creating the application itself, a simple communication protocol was constructed. The communication protocol is relatively straightforward, and the computer application uses 12 sequences to control the device's essential functions. Furthermore, the device usually acknowledges the control sequences by sending back the same or similar message.

Sequence	Request	Acknowledge
L\n	current status of the device	L\n [a]
U\n	0.1 V output voltage increase	U*new_voltage*\n
D\n	0.1 V output voltage decrease	D*new_voltage*\n
E\n	enable the voltage regulator	E\n
F\n	disable the voltage regulator	F\n
B\n	select the big (1 Ω) shunt resistor	B\n
S\n	select the small (10 mΩ) shunt resistor	S\n
A\n	enable the automatic operation	A\n
Q\n	disable the automatic operation	Q\n
O\n	turn-on the display	O\n
P\n	turn-off the display	P\n
M\n	data from the FLASH memory	M\n

[a] followed by respective sequences (regulator enabled and output voltage set to 4 V – send a packet containing E\nU4\n)

Table 4.1: Implemented communication sequences

The sequences shown above are presented in a way that implies the master is the computer, while the device sends only the acknowledgments. However, some of these sequences are bidirectional and are used when the buttons integrated on the PCB are pressed.

The communication also uses three more sequences (4.2); however, these messages are strictly unidirectional, with the device itself always being in a position of a sender.

Sequence	Content	Data structure
"C*data*\n"	measured current reading	16-bit integer
"V*data*\n"	measured voltage reading	12-bit integer
"T*data*\n"	current relative timestamp	16-bit integer

Table 4.2: Unidirectional communication sequences

Furthermore, due to the sheer amount of packets like this, these sequences are not acknowledged.

4.5.3 Computer application

The computer application itself is presented in figure 4.7. It consists of four main sections. The first section, labeled "Connection" provides an option to select the respective virtual COM port and connect to it. Sections labeled "Received data" and "Power consumption" show the received measured data, with average, minimal, and maximal power consumption. These data are then stored and visualized in the "Data visualization" section, where an option between a pure datalog and a chart showing the power consumption is given. All the other sections are used for the control of the device itself.

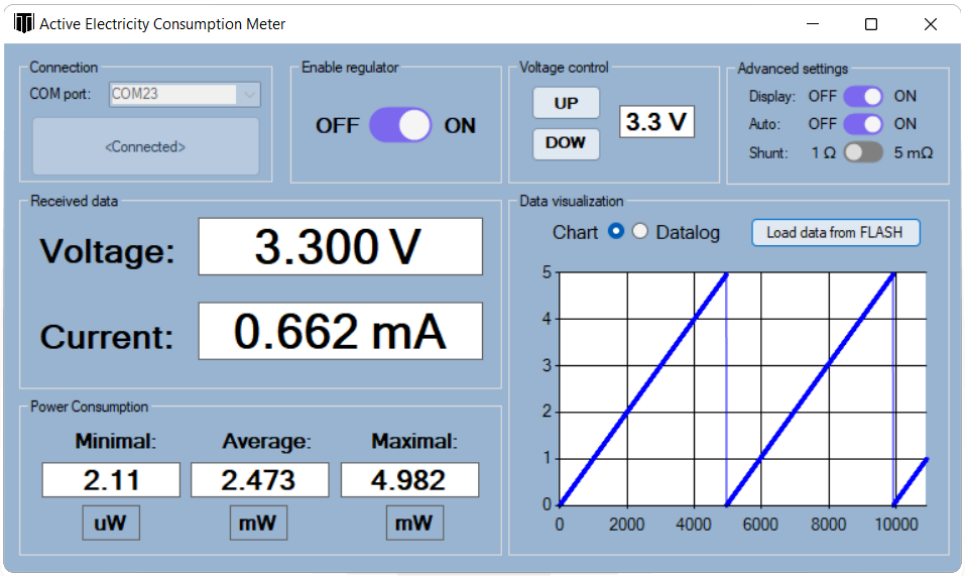

Figure 4.7: Implemented computer application

4.6 Measurements and tests

The last section of this paper focuses on testing of the implemented device. To ensure functionality, multiple tests and measurements were conducted.

In table 4.3, the laboratory equipment utilized for most of the following measurements is presented.

Number	Function	Model and manufacturer
1	Adjustable power supply	KUAIQU SPPS-C3010
2	Function generator	PicoScope 4000A
3	Oscilloscope 1	PicoScope 4000A
4	Oscilloscope 2	TEKTRONIX MDO3014
5	Resistive load - potentiometer	47R, WX903-1

Table 4.3: Utilized laboratory equipment

4.6.1 Oscilloscope connection

To provide an additional option to check and ensure correct functionality, the manufactured board includes a small 3-pin connector (as seen in 4.3) to be used for current sampling by external apparatus. The connector includes:

1. *ADC_IN* signal – analog signal proportional to the drawn current
2. ground connection
3. *MUX_FET* signal – signalizes on which shunt resistor is the measurement taken

As the majority of oscilloscopes nowadays include a math mode, by connecting signal (1) to analog input $A1$ and signal (2) to digital input $D1$, the following equation can be constructed so that signal $I1$ directly corresponds to the output current draw.

$$I1 = (A1 + 99 \cdot D1 \cdot A1)/200 \tag{4.1}$$

4.6.2 Voltage regulator

Besides the design part focusing on the current measurements, a voltage regulator is one of the most important parts of this design. Thus stability and correct functionality of the regulator had to be ensured.

Device start-up

The design of the voltage regulator is presented in 3.3. Because the voltage regulator is controlled and adjusted by the utilized microcontroller, attention to the behavior during the booting sequence should be paid.

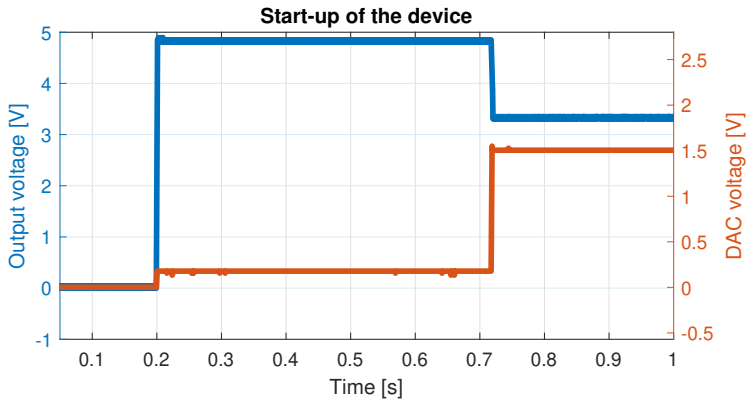

Figure 4.8: Voltage regulator test – device start-up

The measurement can be observed in 4.8 and shows the behavior of the DAC voltage, as well as the output voltage, right after the power is connected. It is evident that the microcontroller takes around 0.7 ms before the pre-programmed DAC output of 1.5 V is seen. This could cause problems when a connected device is not 5 V-tolerant, and is connected during the startup. However, thanks to the connection of the regulator's enable pin to the microcontroller; this issue was mitigated by enabling the regulator only after the DAC signal was ready.

Output voltage adjustment

The adjustment itself is shown in figure 4.9. This test was conducted under no load and clearly shows that the calculated values in 3.9 are nearly identical to the measured data.

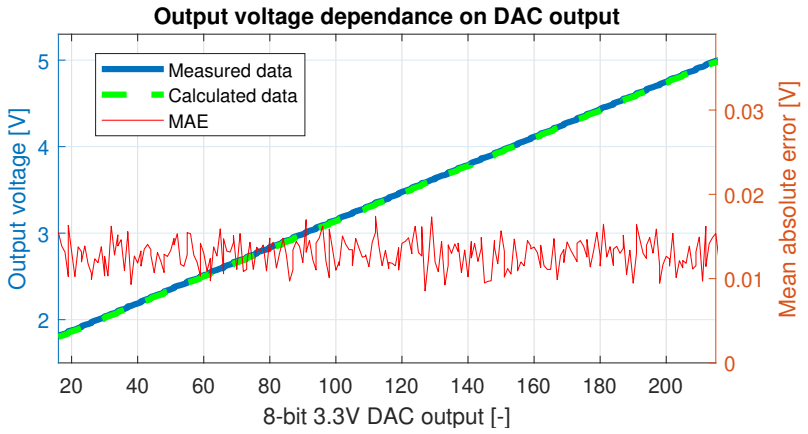

Figure 4.9: Voltage regulator test – voltage adjustment

These data were gathered individually in all 199 points using a 6 1/2 digit voltmeter. The offset of the measured data from the calculated data had a constant nature over the whole range, and the value was approximately V_{off}= 13 mV. The feedback resistors tolerances most likely cause this offset, and thanks to its constant nature, it can be easily suppressed in the software stage. The additional noise present in the MAE calculation is always lower than the DAC's resolution.

Adjustment transient response

To ensure stability during adjustment, the transient response was measured.

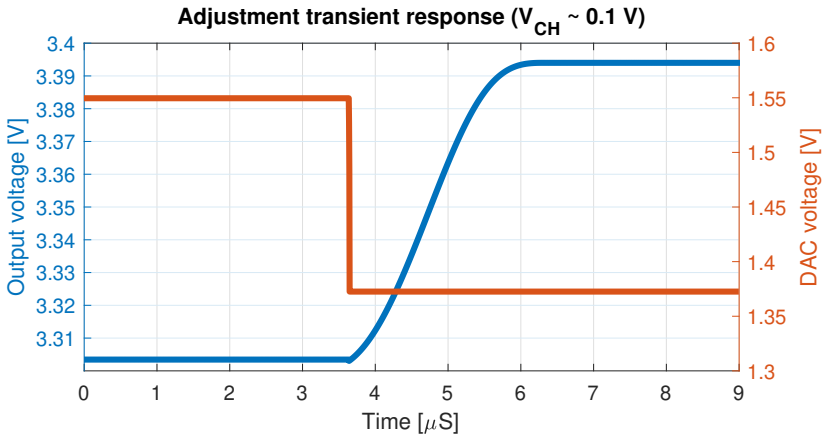

Figure 4.10: Voltage regulator test – adjustment transient response 1

In the graph 4.10 an adjustment with a step of $V_{CH} \sim 0.1\,V$ (corresponds to 0.1 V output voltage change) can be observed. The measurement was taken under no load and shows a fast transient response with a settling time of only around 2 µs and no undershoots or overshoots.

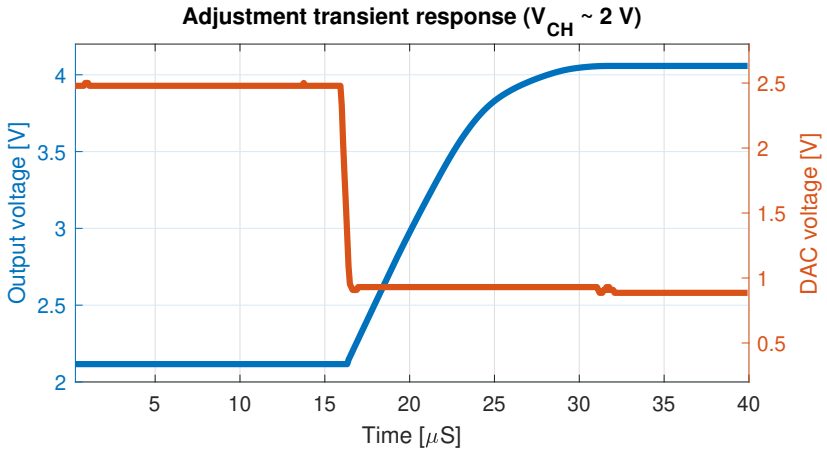

Figure 4.11: Voltage regulator test – adjustment transient response 2

The same measurement under same conditions, but with $V_{CH} \sim 2\,V$ was also taken (4.11). As with the first response, this graph shows a smooth transient response without any overshoots; however, the settling time is much longer with a value of around 15 µs.

Even though both presented responses are measured under no load, similar measurements were taken with a load current $I_{LOAD} = 50\,\text{mA}$ and $I_{LOAD} = 500\,\text{mA}$ and showed almost identical results.

Load transient response

To test the regulator's reaction to a sudden output current change, a $6\,\Omega$ resistive load was connected, resulting in a load current of approximately 550 mA.

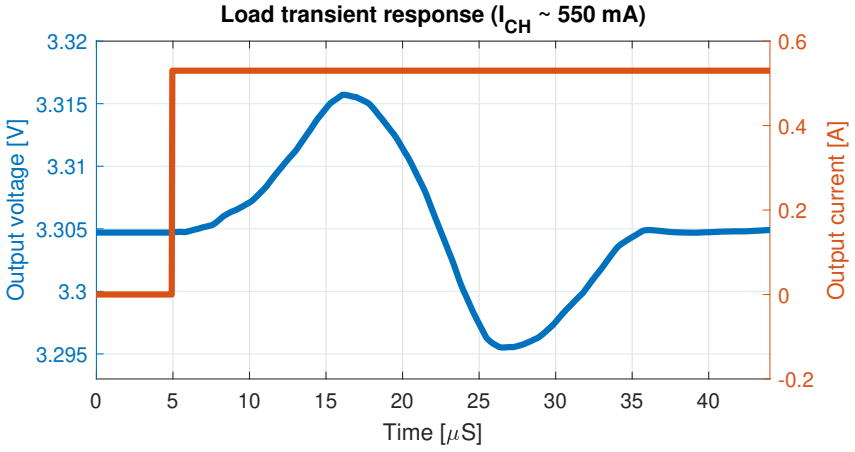

Figure 4.12: Voltage regulator test – load transient response

The maximal output voltage deviance caused by the overshoot/undershoot

was measured as ±11 mV. The measured settling time was 30 µs. Similar behavior was also observed with a sudden drop in the load current.

Load regulation

The load regulation is a measure describing an ability of a power supply to maintain a constant output voltage despite changes in output current or load [79]. Unlike the previous measurements, where an oscilloscope triggering on a rising edge of a respective event was used, the load regulation requires multiple separate measurements. These data were captured in over 100 points, ranging from no load to a maximum load current of 0.5 A, including measurements in µA range. The data points were then interpolated with a second-order polynomial and are shown in 4.13.

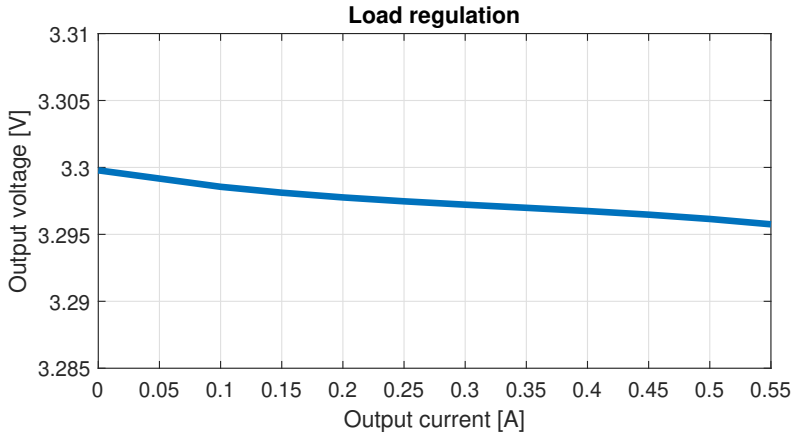

Figure 4.13: Voltage regulator test – load regulation

The output voltage difference between a no-load measurement and a full 0.5 A load measurement was around 4 mV. The regulator's output resistance is thus around 8 mΩ.

Power-supply rejection ratio

The last test regarding the voltage regulator was a measurement of the power-supply rejection ratio. This parameter shows the ability of a regulator to suppress the alternating part of the input supply voltage. Moreover, it determines how effective the regulator is at suppressing the input noise.

To calculate the value, a sine wave with 1 V amplitude was modulated on a 6 V input DC voltage, and the behavior at the regulator's output was observed. The utilized equation is:

$$PSRR = 20 \log(V_{RippleIN}/V_{RippleOUT}) \tag{4.2}$$

However, the PSRR is dependent on many factors, such as input voltage, noise frequency, load current, but also a headroom voltage – the difference between the input and output voltages [80]. Therefore, presenting all this

data in one chart would be either impossible or at least chaotic. For that reason, only measurements under particular circumstances are shown in chart 4.14.

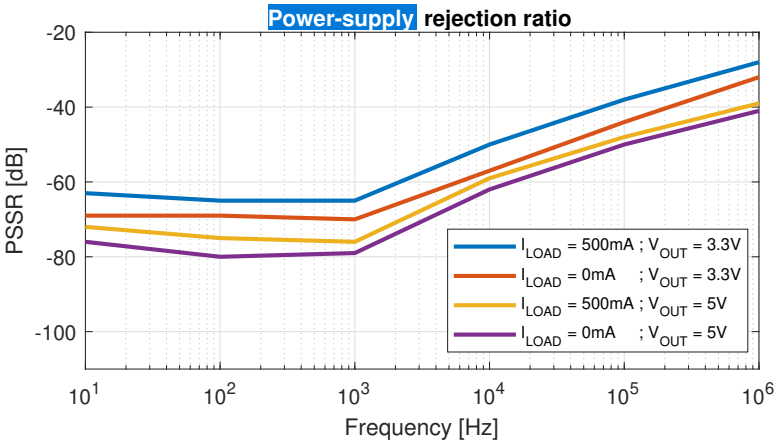

Figure 4.14: Voltage regulator test – power-supply rejection ratio

4.6.3 Current measurements

To test the resolution and accuracy itself, as well as the ability to switch the shunt resistors, multiple tests were conducted. For most of the tests, a sinusoidal or square wave function generator with resistive load was used, generating a current draw with different amplitudes and frequencies.

In each of the following subsections, testing conditions are stated, followed by a respective chart showing the expected waveform and the data sampled by the device. It shall be said that the number of tests was much higher with only a few examples presented in this paper. Secondly, some of the tests utilizing a sine wave may imply that the current is alternating and its direction changes. However, this is not the case and the sine wave was used only to simulate frequent changes in the current draw. The current stays unidirectional over the entire period of the sine wave.

Low frequency and big amplitude

	Signal	Amplitude	Frequency
Test 1	Square wave	0 - 0.46 A	100 Hz

Table 4.4: Current measurements – conditions of test 1

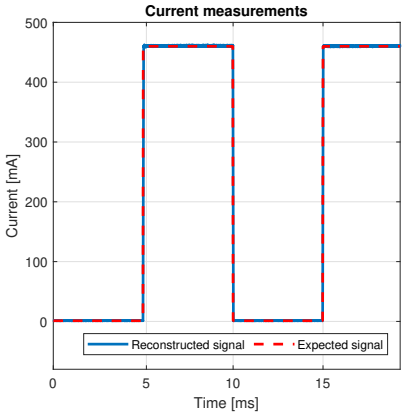

Parameter	Average
MAE (log. 0)	308.79 nA
MAE (log. 1)	347.32 µA
RMSE	148.61 µA
Relative error	1.83 %

(a) : Calculated accuracy

Figure 4.15: Current measurements – test 1

Low frequency and small amplitude

	Signal	Amplitude	Frequency
Test 2	Sine wave	1 µA - 1 mA	100 Hz

Table 4.5: Current measurements – conditions of test 2

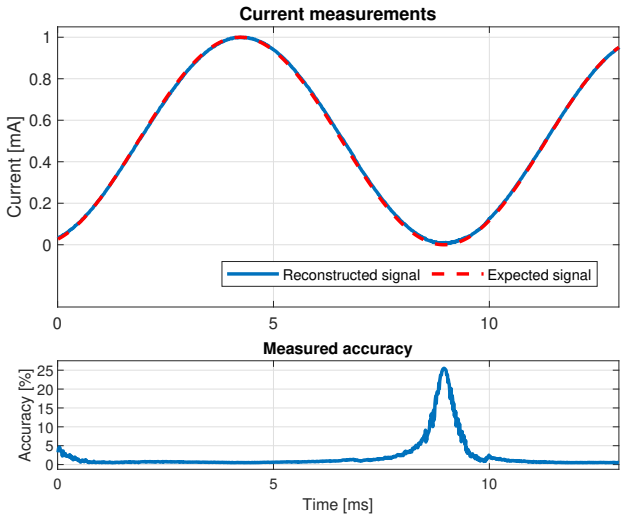

Figure 4.16: Current measurements – test 2

High frequency and low amplitude

	Signal	Amplitude	Frequency
Test 3	Square wave	0 - 5 mA	100 kHz

Table 4.6: Current measurements – conditions of test 3

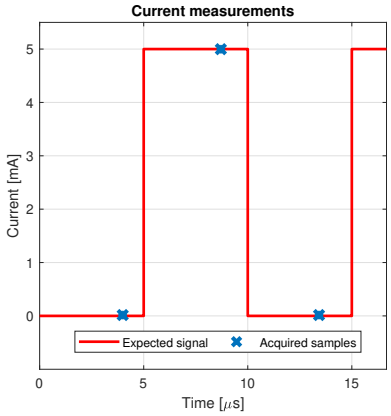

Parameter	Average
MAE (log. 0)	579.12 nA
MAE (log. 1)	4.23 µA
RMSE	3.21 µA
Relative error	4.76 %

(a) : Calculated accuracy

Figure 4.17: Current measurements – test 3

High frequency and big amplitude

	Signal	Amplitude	Frequency
Test 4	Sine wave	0 - 0.1 A	40 kHz

Table 4.7: Current measurements – conditions of test 4

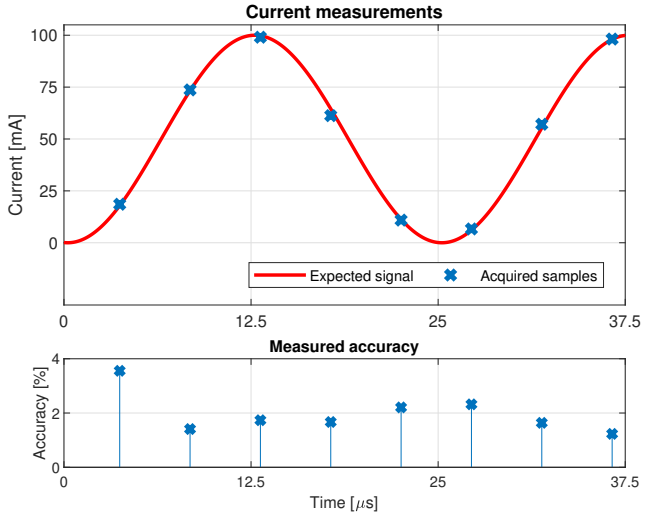

Figure 4.18: Current measurements – test 4

Current shunt switching

In this final test, the correct functionality of the shunt-switching method is presented. Unlike the previous charts, figure 4.19 shows raw ADC output data.

	Signal	Amplitude	Frequency
Test 5	Ramp wave	0 - 30 mA	1 kHz

Table 4.8: Current measurements – conditions of shunt switching test

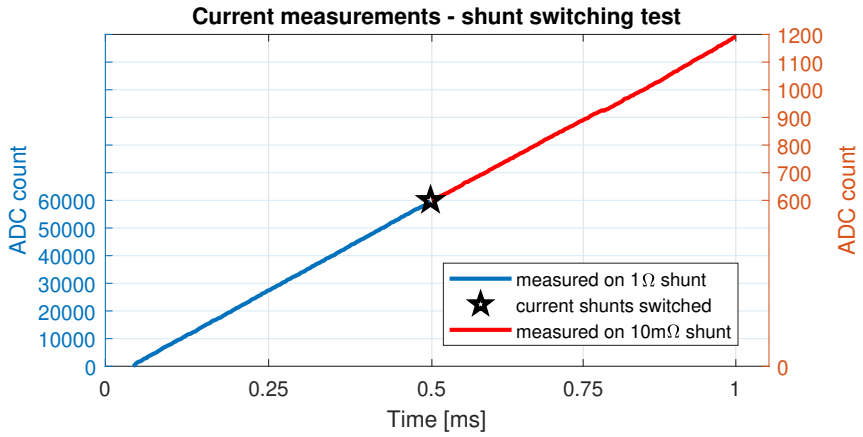

Figure 4.19: Current measurements – shunt switching test

The switching of the shunt resistors can be observed at 0.5 ms, where an ADC output of approximately 60000 (corresponding to a 15 mA current draw) suddenly drops to a 600 – a 15 mA current draw, but measured on the smaller shunt resistor.

Accuracy

The accuracy of the current measurement was closely monitored on numerous tests, while the most significant tests are demonstrated above.

To achieve accurate data, firstly, the input offset voltages of the amplifiers were compensated in the device's software.

To conclude and present some numbers, the final average accuracy of the current measurements was determined. The accuracy is presented as an average relative error of the individual samples from all the conducted tests. The values shown below are separated onto individual shunt resistors, where the measurements were taken.

The accuracy of the current measurements on the bigger (1 Ω) shunt in a range from 1 uA to 15 mA was calculated as:

$$err_{C1\Omega} = 3.42\,\% \tag{4.3}$$

While the accuracy utilizing the smaller (10 mΩ) resistor in a range from 15 mA to 0.5 A shown a value of:

$$err_{C10m\Omega} = 2.64\,\% \tag{4.4}$$

All this current data acquisition, including all the necessary data processing, data transfer, respectively data logging, was achieved with a high sampling rate of approximately:

$$f_s = 212\,000\,\text{Hz} \tag{4.5}$$

While a decrease in accuracy was notable with increasing frequency, an equal number of tests were conducted on various evenly distributed frequencies from 0 to 212 kHz. The error numbers presented above are mean relative errors from all the tests and measurements.

4.6.4 Voltage measurements

As stated in the previous chapters, the voltage is an inherent part of a power consumption calculation; however, in this application, especially since a linear voltage regulator is utilized, the output voltage is generally stable.

This stable behavior was thoroughly observed on many tests and measurements. The biggest overshoots/undershoots were detected during large and high-speed output current peaks (4.12), and even in these conditions, only around 20 µs long deviance were detected. However, in more realistic conditions (extended rise time/more minor current draw change), the deviance was barely noticeable and spanned over only a few microseconds. With the utilized 200 ksps internal ADC, these changes were barely noticeable.

During testing, it had proven much more accurate to utilize averaging methods for power consumption calculations. Thus before every calculation, the output voltage is taken as an average value of the last eight samples taken (if available). Furthermore, when an adjustment request is detected, all the previous samples are discarded.

Steady output voltage

A chart of acquired data, while utilizing the averaging method, is presented in 4.20.

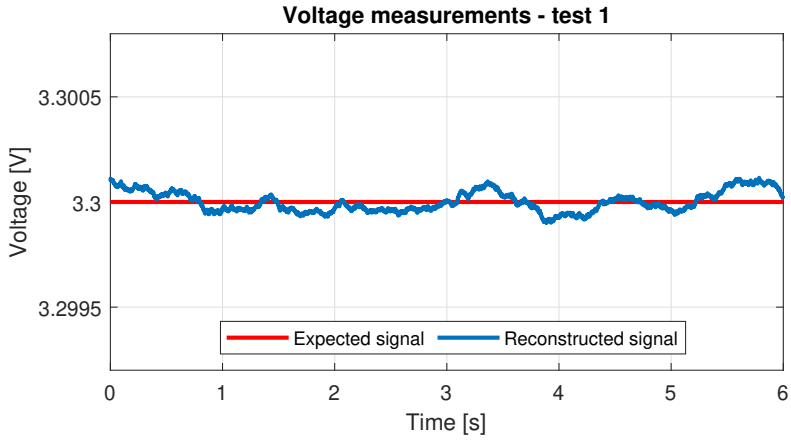

Figure 4.20: Voltage measurements – steady output voltage test

The graph shows that thanks to the averaging, the voltage measurement resolution is higher than the actual resolution of the utilized internal 12-bit ADC. While the 12-bit ADC allows for a resolution of approximately 805 µV, the graph shows a 110 µV maximal deviation from the expected voltage reading.

Voltage adjustment

A test showing the output voltage being gradually adjusted is shown in figure 4.21.

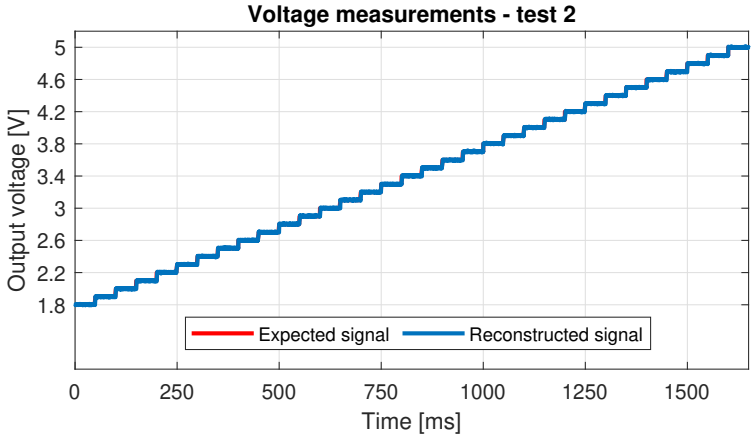

Figure 4.21: Voltage measurements – voltage adjustment test

Accuracy

The overall relative error of the individual voltage samples was calculated as:

$$err_V = 0.72\,\% \tag{4.6}$$

Even though the accuracy seems sufficient, the resolution of the voltage readings proved itself to be the biggest bottleneck of the power consumption calculations.

4.6.5 Power consumption measurement

As the device's primary purpose is to help optimize the power consumption of embedded devices, a final test was conducted. In this scenario, additional ESP32-S2 QT Py was used and connected as a load of the designed device. The measured data are presented in chart 4.22 and their meaning is explained below.

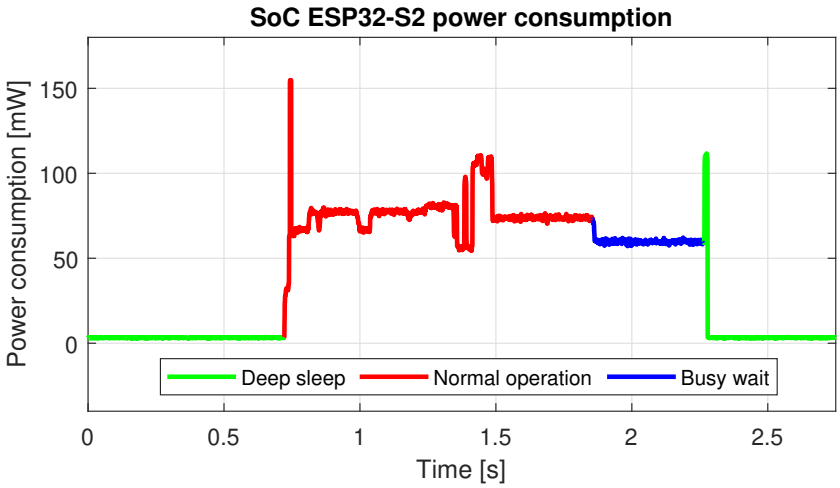

Figure 4.22: SoC ESP32-S2 power consumption

The chart uses three different colors for the respective state the microcontroller is in. While the green color represents deep sleep, the red shows the normal full-speed operation of the monitored device. During normal operation, several GPIOs were toggled, an LED turned on and off and several other primitive functions of the board were tested. Lastly, the blue represents a busy wait – equivalent to a Python function *time.sleep(x)*.

The results clearly state that deep sleep is an efficient way to save power. However, thanks to the fact, that the fast and rather large consumption spikes present while entering, respectively exiting the deep sleep were detected by the designed power consumption meter, an analysis of the deep sleep effectiveness may be considered. While utilizing the deep sleep mode for an extended period of time will surely save power, entering and exiting the deep sleep too often may be counterproductive.

4.7 Device overview

Finally, to summarize, a table containing the essential information about the device is included below (4.9).

Voltage regulator		
Output voltage range	1.8 - 5 V	
Adjustment step size	0.1 V	
Maximal adjustment step error	7.4 mV	
Maximal continuous load current	0.5 A	
Output voltage monitoring		
Sampling frequency	10 kHz [a]	
Measurable range	0 - 5 V	
Relative error	0.72 %	
Load current monitoring		
Sampling frequency	212 kHz	
Measurable range	0 - 1.5 A [b]	
Relative error	[1 µA,15 mA]	(15 mA, 0.5 A]
	3.42 %	2.64 %
Data storage and monitoring		
Onboard stored data	compressed [c]	
Transmitted data (to PC)	all measured data [c]	
PC application monitoring	near real-time [d]	

[a] one voltage sample used for multiple current measurements – resolution and sampling speed subject for future project revisions

[b] only 0.5 A continuous current allowed – peaks up to 1.5 A detectable

[c] only sudden changes stored onboard to allow data storage for longer periods of time – for full resolution, a PC connection is needed

[d] displayed data delayed by processing by around 0.1 s

Table 4.9: Device overview

The designed device with its properties summarized in 4.9 can hardly substitute high-speed oscilloscopes or high-precision voltmeters. However, thanks to its very compact size, affordable price, convenient USB connection, and ability to measure very small and fast power consumption fluctuations, this device may be, for some people, an alternative worth considering. This may include embedded system designers needing to optimize the power consumption of a device, while professional equipment is for them either unaffordable or inconvenient to relocate while moving between places.

Chapter 5

Conclusion

The goal of this project was to design and implement an active power consumption meter that is able to measure fast and small current fluctuations. The main motivation behind this design was to allow embedded design engineers to conveniently and precisely monitor the power consumption and thus help them optimize the power efficiency of future designs. Especially for battery-powered devices, this may often be crucial.

The entire paper is systematically divided into four chapters and serves as a walkthrough of the entire design process. In the beginning, the whole issue is introduced, and many possible design options for every individual part of the design were suggested. After gathering the theoretical information and forming requirements, a circuit schematic was created (6.1). Based on the circuit schematic, a printed circuit board was designed, manufactured, and assembled with respective components. Both sides of the printed circuit board are shown in 6.2 and 6.3. Finally, after programming the device, creating the communication protocol, and implementing a computer application, the device was thoroughly tested via various tests and measurements. These tests were successful, and the results were satisfactory.

To conclude, the paper offers a design solution for a voltage source that provides output voltage between 1.8 V and 5 V with a continuous current draw up to 0.5 A. On top of that, the current draw is constantly monitored with a sampling rate reaching 212 kHz. By utilizing the shunt switching method, the acquired samples showed an average relative error of around 3 %, in a range from 1 µA to 0.5 A. This value, combined with the measured output voltage, is used to calculate average, minimal, and maximal power consumption. The measured and calculated data are then either transferred to a computer via USB or saved to the FLASH memory. Additionally, the data are displayed on display, which is along with the printed circuit board enclosed in a custom 3D printed enclosure.

Even though the assignment was fulfilled, there is plenty of room for future improvement. A major viable improvement would be to utilize a higher quality analog-to-digital converter for the output voltage measurement, which

proved to be the most significant bottleneck in the power consumption calculation. Another significant improvement that was planned, however, due to the time and component shortage constraints not realized, replacing the boost converter with a digitally adjustable buck-boost converter. This addition could lower the power loss on the linear regulator, thus increasing the overall thermal stability, efficiency, and maximal output current. Lastly, the position of current and voltage sensors could be slightly changed, which may increase accuracy by eliminating the ground disturbance and eliminate the need to compensate the measured output voltage for the voltage drop caused by the sense resistors. The last addition utilizing a high-side current sensor is included in the attachments in the form of a block diagram (6.4).

On top of satisfying the assignment, I have gained a lot of new knowledge in circuit design and improved my understanding of voltage regulators and sampling circuits. Moreover, as the design utilized multiple high-speed SPI peripheries, a deep knowledge of high-speed digital layout, as well as techniques like ground splitting, was necessary. Furthermore, the presented design is a third iteration of the design, and each of them brought valuable insight. For example, the first one included a switching regulator as the adjustable regulator, which proved too noisy for the requirements. These iterations and design choices significantly improved my overall circuit design understanding and refined my component parameters and datasheet orientation. Navigating the datasheet was especially important with SPI-controlled devices, where the component's successful operation requires extensive knowledge of its communication protocols, signals, and overall working concept.

The implemented circuit schematics, as well as the printed circuit board gerber files, are included in the attachment section 6.

Bibliography

[1] SAMSUNG. (2022, February 18). *8 tips for maximizing your smartphone battery life.* Samsung Business Insights. https://insights.samsung.com/2022/02/18/8-tips-for-maximizing-your-smartphones-battery-life/

[2] Kastnes, P. (2020, July 29). *Power consumption explained.* Nordic Semiconductor. https://blog.nordicsemi.com/getconnected/power-consumption-explained

[3] Baah, B., & Nwagbo, C. L. (2022). A comparative study of basic types of energy meters and metering. ResearchGate. https://www.researchgate.net/publication/358479054_A_comparative_study_of_basic_types_of_energy_meters_and_metering

[4] Merza, A. M. (2017). Design and Implementation of Prepaid Energy Meter Based on RFID. ResearchGate. https://www.researchgate.net/publication/332142410_Design_and_Implementation_of_Prepaid_Energy_Meter_Based_on_RFID

[5] Khan, S. (2021, December). A comprehensive study on energy meters and power tampering attempts. ResearchGate. https://www.researchgate.net/publication/357318973_A_comprehensive_study_on_energy_meters_and_power_tampering_attempts

[6] Zhang, H. J. (2013, November). *AN-140: Basic Concepts of Linear Regulator and Switching Mode Power Supplies.* Mixed-Signal and Digital Signal Processing ICs ; Analog Devices. https://www.analog.com/en/app-notes/an-140.html

[7] Brown, M. (2001, January). *Power Supply Cookbook.* Elsever. https://www.researchgate.net/publication/277814092_Power_Supply_Cookbook

[8] Khadka, S. K. (2018, February). *Semiconductor Diode, Theory and Principles.* https://www.researchgate.net/publication/323226462_Semiconductor_Diode_Theory_and_Principles

[9] Ain, Q. U., Basim, M., Khan, D., Shehzad, K., Verma, D., & Lee, K.-Y. (2020, June). *A High Power Low Dropout Voltage Regulator Design with an Enhanced Resistive Bank Circuit for Powering an RF IC for DSRC Applications.* https://www.researchgate.net/publication/344204827_A_High_Power_Low_Dropout_Voltage_Regulator_Design_with_an_Enhanced_Resistive_Bank_Circuit_for_Powering_an_RF_IC_for_DSRC_Applications

[10] Stull, R. (2019, December 3). *Isolated vs Non-Isolated Power Converters | CUI Inc. CUI Inc.* https://www.cui.com/blog/isolated-vs-non-isolated-power-converters#benefits-of-isolation

[11] Veerachary, M. (2019, May). *Design and Analysis of Split-Inductor Based Buck-Boost Converters* | IEEE Conference Publication | IEEE Xplore. IEEE Xplore; IEEE. https://ieeexplore.ieee.org/document/8702134

[12] Baba, D. (2011). Isolated Supply Overview and Design Trade-Offs. Texas Instruments.https://www.ti.com/lit/an/snva603/snva603.pdf?ts=1647695465582&ref_url=https%253A%252F%252Fwww.google.com%252F

[13] Husák, M. (2006). *Návrh napájecích zdroju pro elektroniku.*

[14] TEXAS Instruments. (2016, June). *How to Select a Proper Inductor for Low Power Boost Converter.* https://www.ti.com/lit/an/slva797/slva797.pdf?ts=1671969862500

[15] Knight, D. (2016). *Introduction to Linear Voltage Regulators.* DigiKey. https://www.digikey.tw/en/maker/blogs/introduction-to-linear-voltage-regulators

[16] SanBuenaventura, J., & Zhang, H. (2021). *How to Improve Power Supply Output Regulation Accuracy with the LTpowerCAD Resistor Divider Tool* . Analog Devices. https://www.analog.com/en/analog-dialogue/articles/how-to-improve-power-supply-output-regulation-accuracy-with-the-ltpowercad-resistor-divider-tool.html

[17] Texas Instruments. (2014). *TPS65263, 4.5- to 18-V Input Voltage, 3-A/2-A/2-A Output Current Triple Synchronous Step-Down Converter With I2C Controlled Dynamic Voltage Scaling.* https://www.ti.com/lit/ds/symlink/tps65263.pdf?ts=1647700793899&ref_url=https%253A%252F%252Fwww.google.com%252F

[18] Texas Instruments. (2021). *TPS62850x 2.7-V to 6-V, 1-A / 2-A Step-Down Converter in SOT583 Package.* https://www.ti.com/lit/ds/symlink/tps628502.pdf?ts=1647700843059&ref_url=https%253A%252F%252Fwww.google.com%252F

[19] Microchip Technology. (2020). *3A, Power Module Buck Converter with HyperLight Load® Mode and I2C Interface.* https://www.mouser.tw/datasheet/2/268/mchp_s_a0010691121_1-2275316.pdf

[20] Microchip Technology. (2016). *I2C Programmable, 4.5V-19V Input, 5A Step-Down Converter.* https://www.mouser.tw/datasheet/2/268/20005568a-962562.pdf

[21] Maxim Integrated Products. (2002). *Using Digital Potentiometers in Adjustable step-down DC/DC converters design* | Maxim Integrated. https://www.maximintegrated.com/en/design/technical-documents/app-notes/2/225.html

[22] Schweber, B. (2021). *The Fundamentals of Digital Potentiometers and How to Use Them.* DigiKey. https://www.digikey.tw/en/articles/the-fundamentals-of-digital-potentiometers

[23] Glaser, C. (2019). *Methods of output-voltage adjustment for DC/DC converters.* Texas Instruments. https://e2e.ti.com/cfs-file/__key/communityserver-discussions-components-files/196/1373.slyt777_5F00_Methods-of-output_2D00_voltage-adjustment-for-dcdc-converters.pdf

[24] Marcantonio, L. (2021). *Adjusting a fixed-voltage DC/DC converter's output* Electrical Engineering Stack Exchange. https://electronics.stackexchange.com/questions/565430/adjusting-a-fixed-voltage-dc-dc-converters-output

[25] Monolithic Power Systems. (2021). *An Implementation to Adjust ICC with a Digital PWM Signal | Reference Design | MPS.* https://www.monolithicpower.com/en/implementation-to-adjust-icc-with-a-digital-pwm-signal?fbclid=IwAR1J7e0Q1ei5k-ALime_0Ub9OOvjE0kk6dsSNwjZZU3QoJAtXu3ALz1CcHI

[26] Baranov, P. (2015, April 1). *Construction of the coaxial shunt* ResearchGate; Trans Tech Publications, Ltd. https://www.researchgate.net/figure/Construction-of-the-coaxial-shunt_fig1_277663046

[27] Varecha, P., Pacha, M., Sumega, M., & Furmanik, M. (2020, March 1). *Influence of power traces arrangement on quality and reliability of the DC-link current sensing* . ResearchGate; Springer Verlag. https://www.researchgate.net/publication/340015993_Influence_of_power_traces_arrangement_on_quality_and_reliability_of_the_DC-link_current_sensing

[28] Vishay. (2018). *Power Metal Strip® Resistors, Low Value (Down to 0.001), Surface Mount, 4-Terminal.* https://www.vishay.com/docs/30099/wsl3637.pdf

[29] Triano, A. (2014, October). *Choosing the right sense resistor layout.* TI E2E Support Forums. https://e2e.ti.com/blogs_/b/powerhouse/posts/choosing-the-right-sense-resistor-layout

[30] Spaziani, L. (2001). *Using Copper PCB Etch for Low Value Resistance.* Texas Instruments. https://www.ti.com/lit/an/slua236/slua236.pdf?ts=1647766947247&ref_url=https%253A%252F%252Fwww.google.com%252F

[31] Nave, R. (2009). *Hall Effect.*http://hyperphysics.phy-astr.gsu.edu/hbase/magnetic/Hall.html

[32] Schuber, M., Kühne, P., Darakchieva, V., & Hofmann, T. (2016). *Optical Hall effect—model description: tutorial.* Optica Publishing Group. https://opg.optica.org/josaa/fulltext.cfm?uri=josaa-33-8-1553&id=346321

[33] Štindl, D. (2016). *Měření proudu Hallovými senzory.* VUT. Vysoké Učení Technické v Brně. https://www.vutbr.cz/studenti/zav-prace?zp_id=93466

[34] Sonnecy. (n.d.). *SONNECY Closed Loop AC/DC Hall Current Sensor CYHCS-D5S-100A...* Sonnecy Shop. Retrieved March 20, 2022, from https://www.sonnecy-shop.com/en/closed-loop-ac/dc-hall-current-sensor-cyhcs-d5s-100a-output-50ma-100ma-power-supply-12v-18v-window-20mm.html

[35] JSUMO Ultimate robot parts. (n.d.). *ACS770 Hall Effect Current Sensor (ACS770LCB-050U-PFF-T) Current Sensors Allegro | JSumo.com.* Retrieved March 20, 2022, from https://www.jsumo.com/acs770-hall-effect-current-sensor-acs770lcb-050u-pff-t

[36] Palacios, A., In, V., & Longhini, P. (2015, May). *Symmetry-Breaking as a Paradigm to Design Highly-Sensitive Sensor Systems.* Research Gate. https://www.researchgate.net/publication/281662009_Symmetry-Breaking_as_a_Paradigm_to_Design_Highly-Sensitive_Sensor_Systems

[37] Wei, S., Liao, X., Zhang, H., Pang, J., & Zhou, Y. (2021). *Recent Progress of Fluxgate Magnetic Sensors: Basic Research and Application.* MDPI; Multidisciplinary Digital Publishing Institute. https://www.mdpi.com/1424-8220/21/4/1500/htm

[38] Ripka, P., Tipek, A. (2007).*Modern Sensors Handbook.*

[39] Ingenieurbüro Billmann. (n.d.). *Coaxial Shunts. Markus Billmann.* Retrieved March 20, 2022, from http://www.ib-billmann.de/koax_e.php

[40] Stanfel, P., & Morse, M. (2022). *Using a PCB Copper Trace as a Current-Sense Shunt Resistor.* https://www.ti.com/lit/an/sboa533/sboa533.

pdf?ts=1647783783597&ref_url=https%253A%252F%252Fwww.google.com%252F

[41] Yarborough, B. (2020). *Temperature Coefficient of Resistance for Current Sensing.* https://www.vishay.com/docs/30405/whitepapertcr.pdf

[42] Ziegler, S., Woodward, R. C., Iu, H. H.-C., Borle, L. (2009, May 1). *Current Sensing Techniques: A Review.* ResearchGate; Institute of Electrical and Electronics Engineers. https://www.researchgate.net/publication/224393175_Current_Sensing_Techniques_A_Review

[43] IMC-TM. (n.d.). *Measuring currents with extreme dynamics using auto-ranging technology.* Retrieved March 20, 2022, from https://www.imc-tm.com/download-center/white-papers/measuring-currents-with-extreme-dynamics-using-auto-ranging-technology/

[44] Zumbahlen, H. (2008). *Logarithmic Amplifier - an overview.* ScienceDirect. https://www.sciencedirect.com/topics/engineering/logarithmic-amplifier

[45] Analog Devices. (2009). *Log Amp Basics.* https://www.analog.com/media/en/training-seminars/tutorials/MT-077.pdf

[46] Whitehead, A., & Demirci, K. (2020). *Logarithmic Amplifier for Ultrasonic Sensor Signal Conditioning.* Texas Instruments. https://www.ti.com/lit/an/slda053/slda053.pdf?ts=1644763694710&ref_url=https%253A%252F%252Fwww.google.com%252F

[47] Microchip Technology. (2021). *Logarithmic Amplifier.* Microchip Developer Help. https://microchipdeveloper.com/amplifiers:logarithmic-amplifier

[48] Arrow. (2019). *Analog to Digital Converter (ADC) Selection Guide.* Arrow. https://www.arrow.com/en/research-and-events/articles/analog-to-digital-converter-selection-guide

[49] Smith, G. M. (2020, April). *Types of A/D Converters.* Dewesoft. https://dewesoft.com/daq/types-of-adc-converters

[50] Opencircuit. (16 C.E.). *Arduino Nano R3 - clone.* https://opencircuit.shop/product/arduino-nano-r3-clone

[51] Xiangyang, L. (2017, March 17). *Pi Zero.* MakerPro. https://makerpro.cc/2017/03/pi-zero-version-evolution/

[52] Greenfield, D. (2019). *Is Raspberry Pi Ready for Industry?* . Automation World. https://www.automationworld.com/products/control/blog/13319680/is-raspberry-pi-ready-for-industry#:~:text=While%20it%20remains%20true%20that,for%20real%2Dworld%20industrial%20use.

[53] STMicroelectronics. (2021). *STM32H723/733, STM32H725/735 and STM32H730 Value line advanced Arm®-based 32-bit MCUs.* https://www.st.com/resource/en/reference_manual/dm00603761-stm32h723733-stm32h725735-and-stm32h730-value-line-advanced-armbased-32bit-mcus-stmicroelectronics.pdf

[54] EBVElectronic. (n.d.). *STMicroelectronics STM32H723-733 725-735 730 Arm® Cortex®-M7 core.* AVnet. Retrieved March 20, 2022, from https://www.avnet.com/wps/portal/ebv/products/new-products/npi/2020/stmicroelectronics-stm32h723-733-725-735-730/

[55] Espressif Systems. (2021). ESP32-S2 Family. https://www.espressif.com/sites/default/files/documentation/esp32-s2_datasheet_en.pdf

[56] Maxim Integrated. (2001). *Fundamentals of RS-232 Serial Communications .* Maxim Integrated Products. https://www.maximintegrated.com/en/design/technical-documents/tutorials/8/83.html

[57] Sharma, M., Agarwal, N., Reddy, S. R. N. (2015, May). *Design and development of daughter board for USB-UART communication between Raspberry Pi and PC.* ResearchGate. https://www.researchgate.net/publication/308828187_Design_and_development_of_daughter_board_for_USB-UART_communication_between_Raspberry_Pi_and_PC

[58] element14. (n.d.). *FT230XS-R.* Retrieved March 20, 2022, from https://in.element14.com/ftdi/ft230xs-r/i-f-usb2-0-fs-to-basic-uart-16ssop/dp/2081321

[59] Reichelt. (n.d.). *DEBO USB2UART 2 Developer boards - USB type-A to UART, CP2102.* Retrieved March 20, 2022, from https://www.reichelt.com/fr/en/developer-boards-usb-type-a-to-uart-cp2102-debo-usb2uart-2-p266051.html?&nbc=1

[60] Texas Instruments. (2012). *KeyStone Architecture Literature Number: SPRUGP2A March 2012 Serial Peripheral Interface (SPI).* https://www.ti.com/lit/ug/sprugp2a/sprugp2a.pdf?ts=1647665539442&ref_url=https%253A%252F%252Fwww.google.com%252F

[61] Suiu, A. (2020, May 2). *Laboratorul 0xC5: SPI.* Open CourseWare.https://ocw.cs.pub.ro/courses/pm/lab/lab0xc0-6

[62] Tizen. (n.d.). *I2C | Tizen Docs.* Tizen Docs. Retrieved March 20, 2022, from https://docs.tizen.org/iot/guides/peripheral-io-api-i2c/

[63] Infineon Technologies. (2011). *I2C Master/Multi-Master/Slave.* https://www.infineon.com/dgdl/Infineon-Component_I2C_V3.0-Software%20Module%20Datasheets-v03_05-EN.pdf?fileId=8ac78c8c7d0d8da4017d0e952b3f1fbe

[64] Texas Instruments. (2016). *Introduction to the Controller Area Network (CAN).* https://www.ti.com/lit/an/sloa101b/sloa101b.pdf?ts=1647674619135

[65] Texas Instruments. (2004, May). LM2623 General-Purpose, Gated-Oscillator-Based DC-DC Boost Converter. https://www.ti.com/lit/ds/symlink/lm2623.pdf?HQS=dis-mous-null-mousermode-dsf-pf-null-wwe&ts=1662296517280&ref_url=https%253A%252F%252Feu.mouser.com%252F

[66] Texas Instruments. (2015a). *TPS7A45xx Low-Noise Fast-Transient-Response 1.5-A Low-Dropout Voltage Regulators.* https://www.ti.com/lit/ds/symlink/tps7a45.pdf?HQS=dis-mous-null-mousermode-dsf-pf-null-wwe&ts=1648203019734&ref_url=https%253A%252F%252Fwww.mouser.tw%252F

[67] Linear Technology. (n.d.). *LT1965 Series, 1.1A, Low Noise, Low Dropout Linear Regulator.* Analog Technology. Retrieved March 27, 2022, from https://www.mouser.tw/datasheet/2/609/1965fb-1269903.pdf

[68] Diodes Incorporated. (2017). *12V N-CHANNEL ENHANCEMENT MODE MOSFET PowerDI3333-8 (Type UX).* https://www.diodes.com/assets/Datasheets/DMN1004UFV.pdf

[69] Texas Instruments. (2020). *INA281-Q1 AEC-Q100, –4-V to 110-V, 1.3-MHz Current-Sense Amplifier.* https://www.ti.com/lit/ds/symlink/ina281-q1.pdf?ts=1648229345078&ref_url=https%253A%252F%252Fwww.mouser.tw%252F

[70] Texas Instruments. (2005, January). *Single Channel 10-Ohm SPDT analog switch.* https://www.ti.com/general/docs/suppproductinfo.tsp?distId=26&gotoUrl=http%3A%2F%2Fwww.ti.com%2Flit%2Fgpn%2Fts5a2053

[71] Microchip Technology. (2018). *1 Msps/500 kSPS 16/14/12-Bit Single-Ended Input SAR ADC.* https://www.mouser.tw/datasheet/2/268/microchip_technology_mchp-s-a0006919354-1-1749951.pdf

[72] Texas Instruments. (2015b). *TPS731xx Capacitor-Free, NMOS, 150-mA Low Dropout Regulator With Reverse Current Protection.* https://www.ti.com/lit/ds/symlink/tps731.pdf?HQS=dis-mous-null-mousermode-dsf-pf-null-wwe&ts=1648297683249&ref_url=https%253A%252F%252Fwww.mouser.com%252F

[73] Walsh, A. (2012). *Front-End Amplifier and RC Filter Design for a Precision SAR Analog-to-Digital Converter.* Analog Devices. https://www.analog.com/en/analog-dialogue/articles/front-end-amp-and-rc-filter-design.html

[74] Texas Instruments. (2016). *LP2981 100-mA Ultra-Low Dropout Regulators With Shutdown.* https://www.ti.com/lit/ds/symlink/lp2981.pdf?ts=1648205959936&ref_url=https%253A%252F%252Fwww.google.com%252F

[75] Abracon LLC. (2014). *3.3V CMOS SMD Crystal Oscillator.* https://www.mouser.tw/datasheet/2/3/ASEseries-38758.pdf

[76] FTDI. (2005, August). *FT232R USB UART IC Datasheet.* https://www.mouser.tw/datasheet/2/163/DS_FT232R-11534.pdf

[77] Adafruit Industries. (n.d.). *Adafruit QT Py - SAMD21 Dev Board with STEMMA QT: ID 4600* Adafruit Industries. Retrieved March 27, 2022, from https://www.adafruit.com/product/4600

[78] Sparkfun. (n.d.). Adafruit Industries. (n.d.-a). *Adafruit Grayscale 1.5 128x128 OLED Graphic Display [STEMMA QT / Qwiic].* Adafruit Industries. Retrieved May 3, 2022, from https://www.adafruit.com/product/4741

[79] Sunpower electronics. (n.d.). *Load Regulation.* Retrieved May 3, 2022, from https://www.sunpower-uk.com/glossary/what-is-load-regulation/#:~:text=Load%20regulation%20is%20the%20measure,to%20the%20circuit%20or%20system.

[80] Morita, G. (n.d.). *LDO Operational Corners: Low Headroom and Minimum Load.* Analog Devices. Retrieved May 3, 2022, from https://www.analog.com/en/analog-dialogue/articles/ldo-operational-corners.html

Chapter 6

Attachments

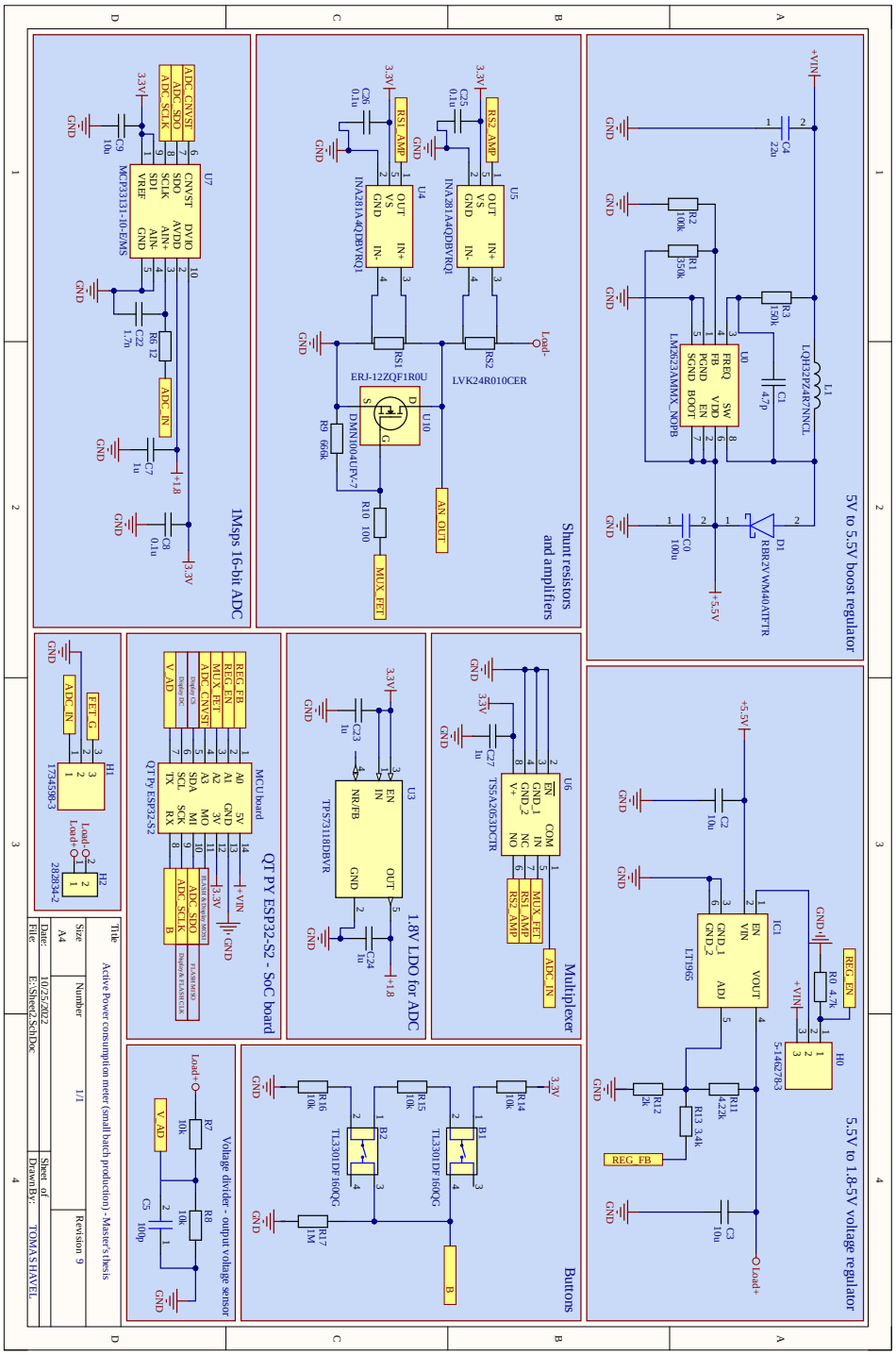

Figure 6.1: Complete circuit schematic

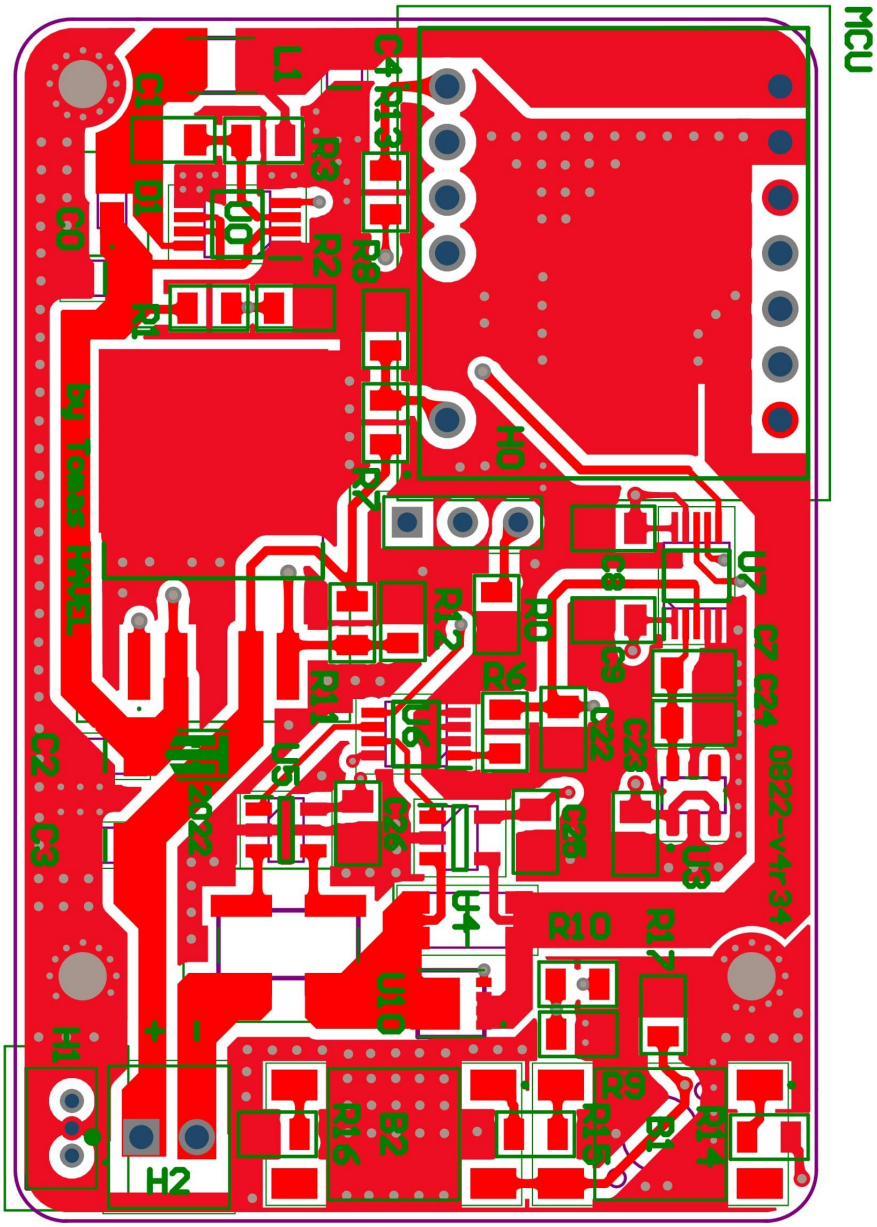

Figure 6.2: PCB top layer

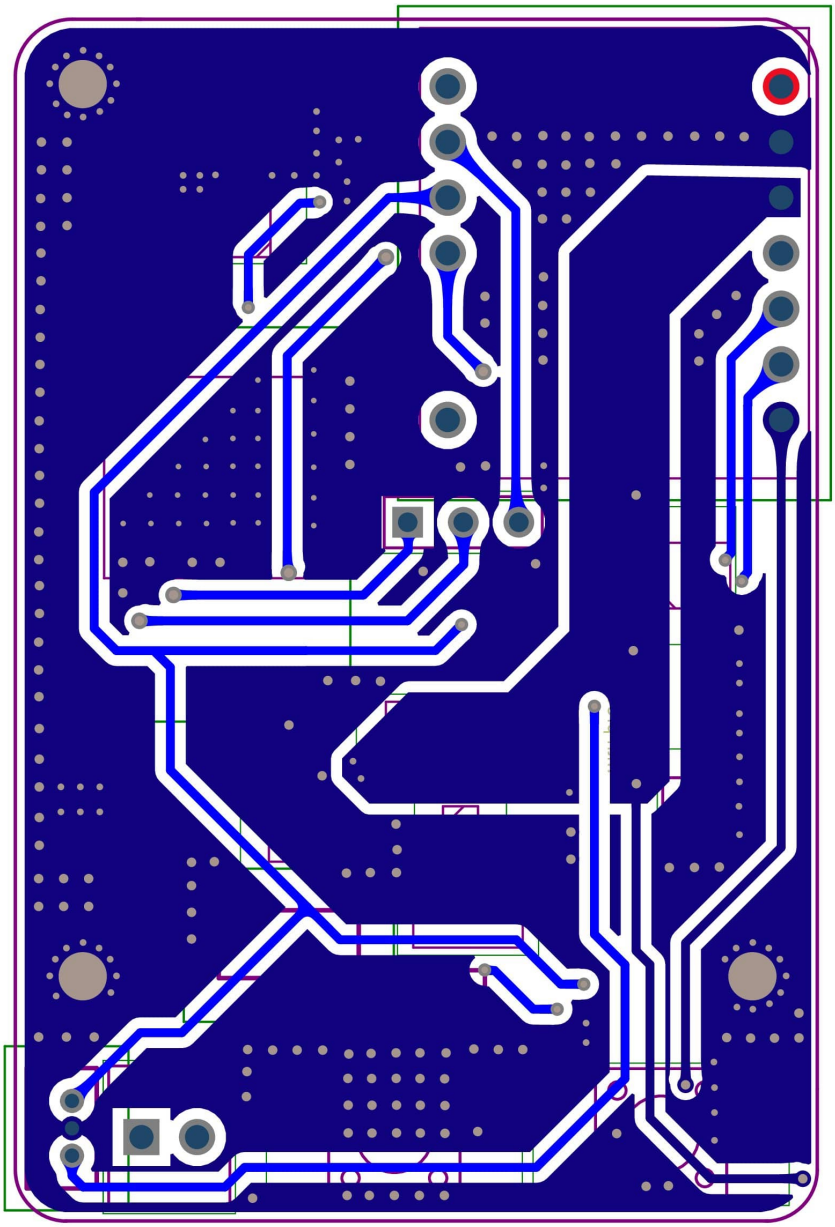

Figure 6.3: PCB bottom layer

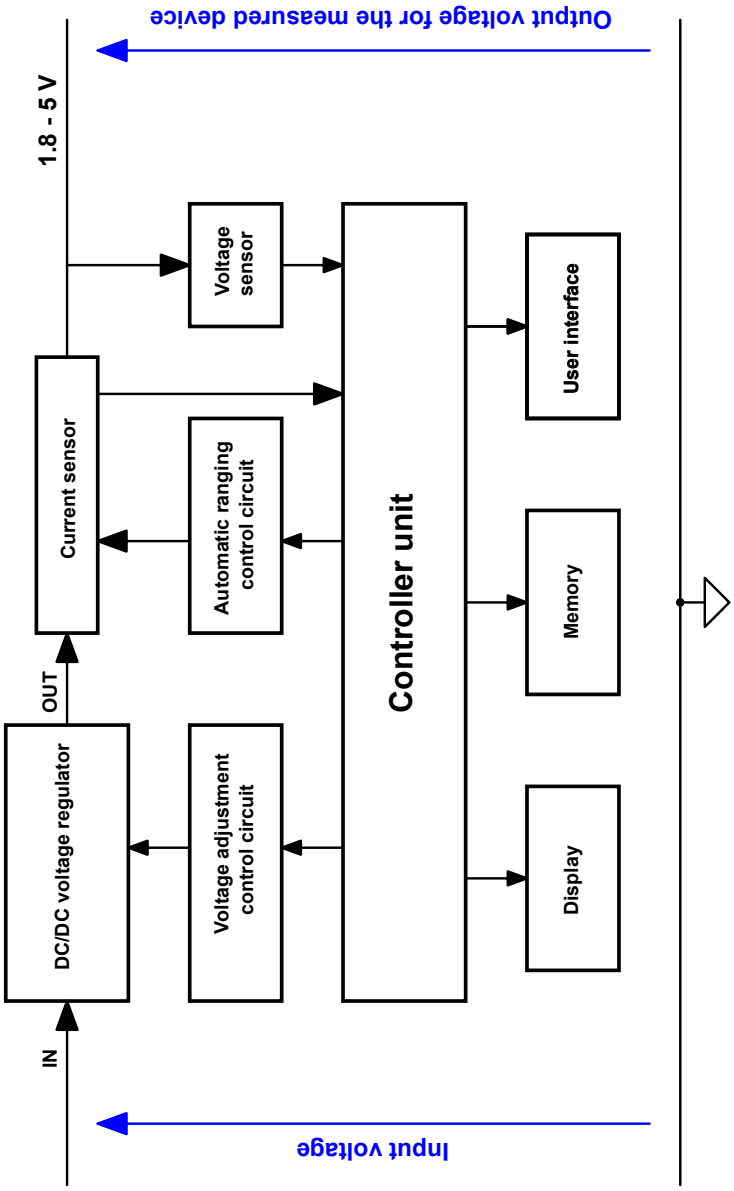

Figure 6.4: Possible future improvement - high-side current sensing